Coupled whole-tree optimality and xylem hydraulics explain dynamic biomass partitioning

Aaron Potkay[1] (iD), Anna T. Trugman[2] (iD), Yujie Wang[3,4] (iD), Martin D. Venturas[3] (iD), William R. L. Anderegg[3] (iD), Caio R. C. Mattos[1] and Ying Fan[1] (iD)

[1]Department of Earth and Planetary Sciences, Rutgers University, New Brunswick NJ 08854, USA; [2]Department of Geography, University of California, Santa Barbara, Santa Barbara CA 93106, USA; [3]School of Biological Sciences, University of Utah, Salt Lake City UT 84112, USA; [4]Division of Geological and Planetary Sciences, California Institute of Technology, Pasadena CA 91125, USA

Summary

- Trees partition biomass in response to resource limitation and physiological activity. It is presumed that these strategies evolved to optimize some measure of fitness. If the optimization criterion can be specified, then allometry can be modeled from first principles without prescribed parameterization.
- We present the Tree Hydraulics and Optimal Resource Partitioning (THORP) model, which optimizes allometry by estimating allocation fractions to organs as proportional to their ratio of marginal gain to marginal cost, where gain is net canopy photosynthesis rate, and costs are senescence rates. Root total biomass and profile shape are predicted simultaneously by a unified optimization. Optimal partitioning is solved by a numerically efficient analytical solution.
- THORP's predictions agree with reported tree biomass partitioning in response to size, water limitations, elevated CO_2 and pruning. Roots were sensitive to soil moisture profiles and grew down to the groundwater table when present. Groundwater buffered against water stress regardless of meteorology, stabilizing allometry and root profiles as deep as *c.* 30 m.
- Much of plant allometry can be explained by hydraulic considerations. However, nutrient limitations cannot be fully ignored. Rooting mass and profiles were synchronized with hydrological conditions and groundwater even at considerable depths, illustrating that the below ground shapes whole-tree allometry.

Introduction

Forests store *c.* 45% of terrestrial carbon (Sabine *et al.*, 2004) and sequester large amounts of carbon annually (Bonan, 2008; Beer *et al.*, 2010; Pan *et al.*, 2011). The terrestrial biosphere has drawn down around one-third of anthropogenic CO_2 emissions since the beginning of the industrial era and thereby suppressed climate change (Le Quéré *et al.*, 2018). Yet, it remains unclear how the terrestrial carbon sink's strength will respond to climate change (Ballantyne *et al.*, 2015; Schimel *et al.*, 2015), particularly the combination of elevated atmospheric CO_2, warmer temperatures and more severe drought (Sperry *et al.*, 2019). Carbon-allocation strategies of trees, referring here to the dynamic biomass partitioning between organs, plays a critical role in carbon exchange between the atmosphere and the biosphere (Litton *et al.*, 2007; Bonan, 2015). Allocation is shaped by intrinsic plant physiological traits, competition, and the local environment (Poorter & Nagel, 2000; Poorter *et al.*, 2012). However, mechanistic vegetation models that predict responses to changes in CO_2 and climate often predict tree allometry using fixed ratios or scaling laws, despite the fact that these approaches do not capture known carbon allocation dynamics and responses to

environmental conditions and stand age (Drewniak & Gonzalez-Meler, 2017; Merganičová *et al.*, 2019; Xia *et al.*, 2019; Trugman *et al.*, 2019a).

Plants partition biomass in response to resource limitation and the physiological activity of each organ according to functional equilibrium (Brouwer, 1962, 1963). Functional equilibrium is grounded in observations that plants shift allocation towards shoots if fitness is impaired by uptake of above-ground resources (light and atmospheric CO_2; but see Stulen & Hertog, 1993, Poorter & Nagel, 2000, and Poorter *et al.*, 2012, for contradicting evidence regarding CO_2; Fig. 1). Similarly, plants shift allocation towards roots when fitness is limited by uptake of below-ground resources (water and nutrients; Aber *et al.*, 1985; Gower *et al.*, 1992; Jiménez *et al.*, 2009). Plant allometry changes dramatically with resource availability in general agreement with functional equilibrium (Poorter & Nagel, 2000), and size- or age-dependent changes in resource use generate coinciding changes in allometry consistent with functional equilibrium (Buckley & Roberts, 2006b; Poorter et al., 2012). Additionally, water transport through xylem may limit productivity, because water loss through stomata must balance water supplied by the hydraulic continuum (Sperry & Love, 2015; Sperry *et al.* 2016),

and thus hydraulic resistances throughout the plant should be finely balanced to optimize transpiration (Magnani et al., 2000), shown by near-equal proportioning of above- and below-ground hydraulic resistances in trees (Landsberg et al., 1976; Roberts, 1977; Running, 1980; Irvine & Grace, 1997; Tsuda & Tyree, 1997; Martínez-Vilalta et al., 2007; Poyatos et al., 2018).

Optimal plant function modeling captures functional equilibrium with fewer parameters compared with empirical and more mechanistic approaches. They predict allometry by optimizing a goal or objective function, which is often growth or canopy assimilation rates (Dewar et al., 2009; Anten & During, 2011; Franklin et al., 2012) and occasionally reproductive fitness (Dybzinski et al., 2011, 2014; Farrior et al., 2013). They have explained changes in allometry as a result of size (Buckley & Roberts, 2006a,b), elevated atmospheric CO_2 (Franklin, 2007), nutrient supply (Mäkelä et al., 2008), changes in both CO_2 and nutrient uptake (McMurtrie et al., 2008; Thornley & Parsons, 2014; Dybzinski et al., 2015), and precipitation gradients (Yang et al., 2018) and hydrological seasonality (Farrior et al., 2013). However, optimality has yet to be extensively shown to explain
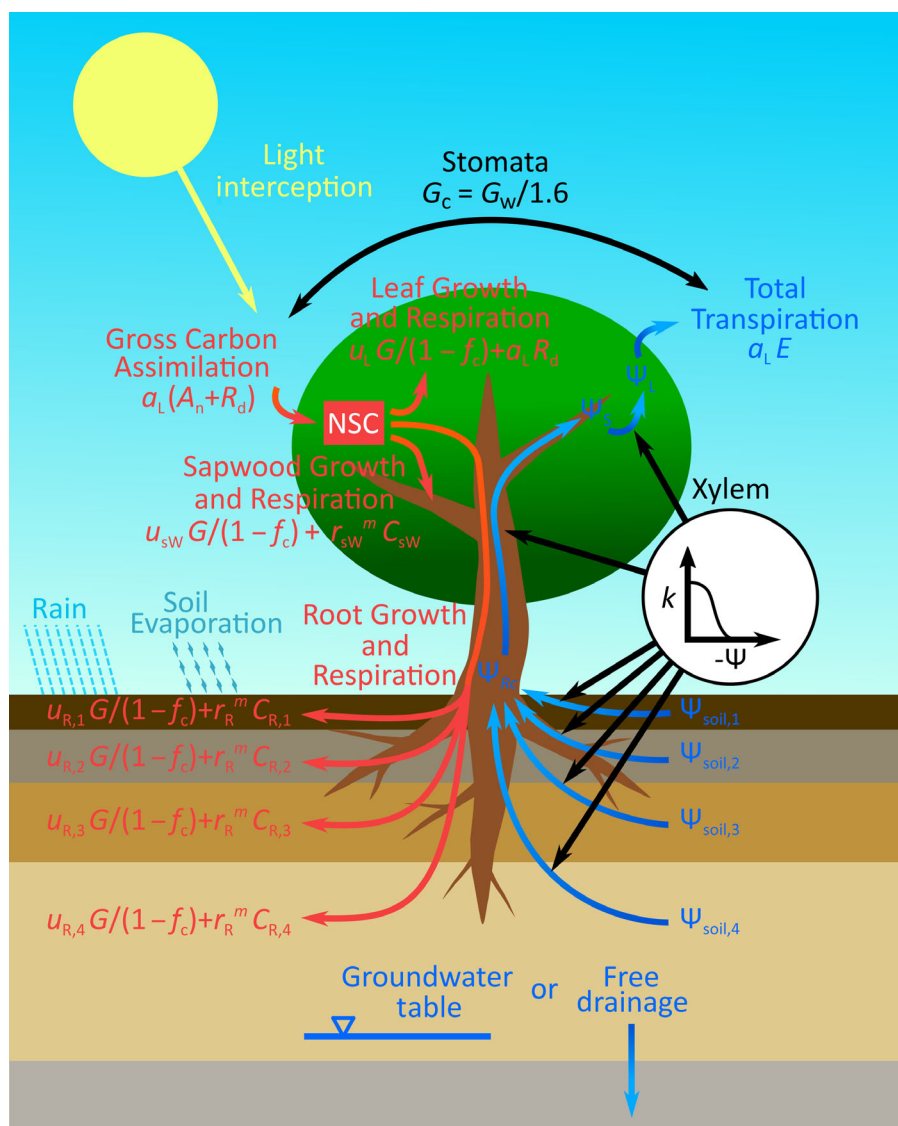

Fig. 1 Conceptual diagram for the Tree Hydraulics and Optimal Resource Partitioning (THORP) model (see Supporting Information Table S1 for symbols used). Soil hydrology is simulated by the Richards equation from precipitation, soil evaporation, transpiration, and either a shallow groundwater or free drainage lower boundary condition. Roots conduct water from their soil layers according to the layer's composite soil–root conductance and the gradient between soil water potential, Ψ_{soil}, and root collar xylem potential, Ψ_{Rc}. The total transpiration is conducted through stems and then leaves, which are given by their conductances, k, and stem apex and leaf xylem potentials, Ψ_S and Ψ_L. Root, stem and leaf conductances depend on the size of each structural carbon pool, C_R (roots), C_{sW} (sapwood) and C_L (leaf; or more accurately leaf area, a_L), and may decline as a result of xylem embolism. Transpiration and carbon assimilation rates, E and A_n, are linked through stomata, which respond to water stress and light interception. Assimilated carbon is added to a nonstructural carbon (NSC) pool, where it is available for growth, G, and maintenance ($r_R{}^m C_R$ for roots, $r_{sW}{}^m C_{sW}$ for sapwood, and $a_L R_d$ for leaves, where R_d is the leaf dark respiration) and construction respiration, the latter of which is represented as a fixed fraction, f_c, of growth. THORP predicts the dynamic carbon allocation fraction to the ith structural carbon pool, u_i, that optimizes net assimilation depending on the tree's resource needs and ability to improve water use and light interception.

whole-tree allometry under other environmental conditions, particularly water stress (see Givnish, 1986; Sperry *et al.*, 2019; Trugman *et al.*, 2019a,b for reduced leaf biomass under water stress). Many optimal function models are static and describe growing season averages rather than dynamic growth or short-term fluctuations. As these models have not been designed to simulate short-term responses to water stress, they lack mechanistic representations of xylem hydraulics. Instead, xylem water potentials have been fixed (Buckley & Roberts, 2006a,b), annual transpiration has been a fraction of annual rainfall that is either fixed (McMurtrie *et al.*, 2008) or an empirical function of leaf area index (LAI; Yang *et al.*, 2018), or hydraulic limitations have been ignored and photosynthesis is modeled independently of stomatal behavior (Franklin, 2007; Mäkelä *et al.*, 2008; Thornley & Parsons, 2014).

Here, we present a new model, Tree Hydraulics and Optimal Resource Partitioning (THORP), which predicts the dynamic partitioning of an individual tree's biomass among stems, roots and leaves that optimizes net assimilation. This optimization results in the greatest growth in the most limiting organ in agreement with functional equilibrium. The tree is ever-striving towards an optimal allometry that balances whole-tree water use and light interception, depending dynamically on the environment and its structure and physiology. Each organ competes for carbon until a hydraulic balance is achieved and no one organ is limiting transpiration. Similar to previous models of root traits (Table 1), THORP preferentially grows roots at depths where the benefits to transpiration are greatest based on the spatial distribution of soil moisture, the conductances along the soil–root hydraulic pathway at each depth, and the vertical distance between root tip and collar. Few other models capture root biomass, depth and shape simultaneously (Table 1). THORP is the only model to our knowledge that applies the organizing principle of optimality to predict all three root traits in unison. Like THORP, other models that predict root biomass through optimality (Givnish, 1986; Magnani *et al.*, 2000; Schwinning & Ehleringer, 2001; Buckley & Roberts, 2006a) consider the whole-tree balance of hydraulic resistances, thereby integrating below- and above-ground allocation. These optimality models, however, have not mechanistically described soil moisture dynamics, which control depths and profiles in other stochastic and multilayered water-balance models. THORP attempts to unify whole-tree optimality and water-balance approaches.

THORP is coupled to Sperry *et al.*'s (2017) gain–risk optimization algorithm to estimate transpiration rates, soil drying, the water-use efficiency of stomata, and the conductances throughout the tree which inform THORP how best to invest carbon between organs. The gain–risk algorithm has been validated at the individual plant level in garden experiments (Venturas *et al.*, 2018; Wang *et al.*, 2019) and at the ecosystem level (Sabot *et al.*, 2020). Carbon partitioning in THORP is solved analytically and is a dynamic product of environmental and physiological conditions without model parameters that explicitly control allometry. Unlike previous optimal growth models which are too computationally complex for large-scale vegetation modeling (Merganičová *et al.*, 2019), THORP's analytical framework

for allocation is numerically efficient and appropriate for future integration into such models. THORP's optimality approach reduces the number of poorly constrained parameters compared with traditional carbon allocation models (Trugman *et al.*, 2019b). As large-scale vegetation models already simulate many of THORP's underlying processes, recently including xylem hydraulics (Christoffersen *et al.*, 2016; Eller *et al.*, 2020; Sabot *et al.*, 2020), integration would require no new parameters. Large-scale application of THORP would likely be done in a simplified form after further validation, much as Sperry *et al.*'s (2017) gain–risk optimization algorithm was simplified for ecosystem-level simulations (Sabot *et al.*, 2020).

Foremost, we hypothesize that much of carbon allocation is driven to meet hydraulic demands. This hypothesis is a key assumption of THORP's framework that we test here and which differs from previous optimal plant function models, which often predict an allometry that solely considers the tradeoffs among concentrating foliar nutrients, canopy size and respiration (Franklin, 2007; Mäkelä *et al.*, 2008; McMurtrie *et al.*, 2008) but not water use. We test this hypothesis by developing THORP, which focuses on balancing internal hydraulic resistances without explicit consideration of nutrient demands, and demonstrating that THORP predicts reported trends in the biomass partitioning of trees as a function of size and in response to various environmental conditions: light and water limitations, elevated CO_2 (eCO_2) and pruning.

Following our first hypothesis that hydraulic demands play a critical role in allocation, soil hydrology, which sets in motion the transpirational stream, should govern much of allocation. We apply THORP to test an additional hypothesis of soil hydrology's role. Our second hypothesis is that trees modulate their rooting depth and profiles in synchrony with hydrological conditions. We expect that rooting distributions are sensitive to hydrometeorological conditions in solely rain-fed environments, where root profiles vary dynamically to follow seasonal changes in soil moisture distribution (Chen *et al.*, 2004). Where groundwater is shallow, we expect rooting depth to follow the water table independently of meteorology (Naumburg *et al.*, 2005; Christina *et al.* 2017; Fan *et al.*, 2017). Following from this second hypothesis, we expect that access to stable sources of deep soil moisture or shallow groundwater will allow trees growing under reduced precipitation to partition biomass as if not droughted. Access to steady soil water and groundwater would fulfill a tree's hydraulic needs even under declining precipitation, meaning that less biomass should be allocated below ground for above- and below-ground resource uptake to equally limit fitness (Bloom *et al.*, 1985). Soil water and groundwater access organizes tree hydraulic properties (Alder *et al.*, 1996; Carter & White, 2009; Zolfaghar *et al.*, 2015) and alleviates mortality under meteorological drought (Tai *et al.*, 2018; Love *et al.*, 2019; Mackay *et al.*, 2020; McLaughlin *et al.*, 2020). However, groundwater's role in tree allometry has only recently been recognized (Carter & White, 2009; Zolfaghar *et al.*, 2014, 2015), often with emphasis on above-ground allometry (e.g. sapwood–-leaf relations), while few groundwater studies consider both above- and below-ground biomass (Imada *et al.*, 2008; Xu *et al.*,

Table 1 Select models, their ability to capture rooting depth, root biomass and shape of root profile with depth, and whether they simulate dynamic, vertically explicit soil moisture profiles.

Reference	Model	Underlying principle	Root biomass?	Rooting depth?	Rooting profile?	Realistic soil hydrology?
Givnish (1986)	–	Optimizes net carbon gain	Y	N	N	N
Kleidon & Heimann (1996)	–	Optimizes transpiration (further constrained by carbon costs)	Y[1]	Y	Y	Y[2]
Magnani et al. (2000)	–	Optimizes net carbon gain	Y	N	N	N
Van Wijk & Bouten (2001)	SWIF	Optimizes transpiration	N	Y	Y	Y
Schwinning & Ehleringer (2001)	–	Optimizes net carbon gain	Y	N	Y	N[3]
Buckley & Roberts (2006a)	DESPOT	Optimizes net carbon gain	Y	Y	N	N
Laio et al. (2006)	–	Imposes that long-term mean soil moisture will be vertically homogeneous	N	Y	Y	Y[2,4]
Collins & Bras (2007)	–	Optimizes transpiration	N	Y	Y	Y[2]
Guswa (2008)	–	Optimizes net carbon gain	N	Y	N	Y[2,4]
Schenk (2008)	SWIEM	Shallowest possible profile	N	Y	Y	Y[2]
Schymanski et al. (2008, 2009)	–	Preferential root growth where root water uptake is high and to maintain root tissue water storage	Y[5]	Y	Y	Y
Sivandran & Bras (2013)	VEGGIE	Optimizes transpiration	Y[6]	Y	Y	Y[2]
Fan et al. (2017)	LEAF-Hydro-Flood	Preferential rooting where hydraulic resistances are least	N	Y	Y	Y
Mackay et al. (2020)	TREES	Preferential root growth where hydraulic conductances are high and where senescence costs are low	Y	N	Y	Y
Present study	THORP	Optimizes net carbon gain	Y	Y	Y	Y

DESPOT, Deducing Emergent Structure and Physiology Of Trees; LEAF, Land-Ecosystem-Atmosphere Feedback; SWIEM, soil water infiltration and extraction model; SWIF, Soil Water In Forested ecosystems; TREES, Terrestrial Regional Ecosystem Exchange Simulator; THORP, Tree Hydraulics and Optimal Resource Partitioning model; VEGGIE, Vegetation Generation for Interactive Evolution

[1]Kleidon & Heimann (1996) model the change in root biomass as a constant growth rate, rather than predict it by optimality.

[2]Study does not consider possibility of groundwater. While the models by Kleidon & Heimann (1996), Collins & Bras (2007) and Sivandran & Bras (2013) were run with a free-drainage lower-boundary condition, groundwater could conceivably be added to their existing frameworks, as these models solve the Richards equation or a similar diffusion-type equation for soil moisture dynamics. This possibility of groundwater representation is not possible in other models based on stochastic rainfall without significant model changes.

[3]Schwinning & Ehleringer (2001) model two soil layers; however, the two layers do not exchange water. The bottom layer is held at constant soil water potential, while soil moisture in the top layer responds to water inputs and drying through evapotranspiration.

[4]Soil moisture predicted solely from stochastic representation of precipitation and infiltration.

[5]Schymanski et al. (2008, 2009) do not model change in root biomass through optimality; instead, within a soil layer, root growth rate is treated as a function of root water uptake within that soil layer and thus ignores above-ground processes in the whole-tree carbon balance (e.g. photosynthesis, shoot allocation, etc.).

[6]Root allocation in VEGGIE is not based on optimality but on a resource limitation approach (Arora & Boer, 2005; Ivanov et al., 2008), which has been suggested to perform inadequately in model–data comparisons (De Kauwe et al., 2014; Xia et al., 2019).

2017). Few studies have simulated both below- and above-ground allocation changes as a result of groundwater (e.g. Mackay et al., 2020) as achieved by THORP. Thus, groundwater influence may be under-predicted by many large-scale land models that do not represent groundwater (Clark et al., 2015; Fan et al., 2019) or its potential influence on vegetation, despite the fact that shallow groundwater may influence much of the global land area (Fan et al., 2013, 2017).

Materials and Methods

Model description

Here, we summarize THORP's core assumptions, structure (Fig. 1 See later; Supporting Information Fig. S1; Notes S1) and main variables (Table S1). Photosynthesis is calculated with a big-leaf version of the Farquhar et al. (1980) model, based on electron transport and carboxylation capacities, photosynthetic irradiance and stomatal conductance (Notes S1 S.6). Light interception is canopy-averaged from total light capture, which is calculated by the Beer-Lambert law, for a spatially uniform leaf distribution (Notes S1 S.5). Sperry et al.'s (2017) gain–risk algorithm predicts stomatal conductance and xylem water potentials from environmental factors (e.g. soil drying, vapor pressure deficit, temperature, photosynthetic active radiation, atmospheric CO_2 concentrations; Notes S1 S.6). Assimilated carbon is added to a nonstructural carbohydrate (NSC) storage pool, which is depleted by maintenance and construction respiration and growth (Notes S1 S.9). Maintenance respiration is temperature-dependent and calculated independently for each structural carbon pool (Notes S1 S.7). Construction respiration rates are proportional to growth rates (Notes S1 S.9). Growth rates are not directly coupled to photosynthesis (Fatichi et al., 2014; Merganičová et al., 2019) and instead depend on NSC storage

(Schiestl-Aalto *et al.*, 2015; Hayat *et al.*, 2017; Notes S1 S.9), enabling THORP to capture recovery processes after disturbances (Barigah *et al.*, 2013; Hartmann, 2015). Root, leaf and sapwood pools acquire carbon through growth and lose carbon through senescence, which is modeled by mean life spans (Notes S1 S.7). Senesced sapwood becomes heartwood (Notes S1 S.9). Changes in the sizes of carbon pools cause changes in leaf area, tree height, canopy width, basal diameter and the root distribution with soil depth (Notes S1 S.1), which influence how efficiently the tree intercepts light (Notes S1 S.5), transpires water (Notes S1 S.3), and thus photosynthesis. Height and canopy width are constrained by basal diameter according to power laws (McMahon, 1973; West *et al.* 1999, 2009; Niklas & Spatz, 2004; Notes S1 S.1), and stem conductance is similarly dependent on tree size according to a fractal-like hydraulic tree architecture and sapwood and heartwood proportions (West *et al.*, 1999; Savage *et al.*, 2010; Sperry *et al.* 2012; Hölttä *et al.*, 2013; Notes S1 S.4).

Distributions and dynamics of soil moisture with depth are solved numerically by the one-dimensional vertical form of Richards equation (Richardson, 1922; Richards, 1931) (Notes S1 S.2). Soil porosity and hydraulic conductivity decline exponentially with depth (Beven & Kirkby, 1979; Fan *et al.*, 2013), and unsaturated soil hydraulic properties are modeled after van Genuchten (1980). Infiltration rates are assumed equal to precipitation, and soil evaporation is modeled by a linearized form of Dalton's law of evaporation (Penman, 1948). Transpired water is removed from each soil layer according to water potential gradients and hydraulic resistances along the soil–root pathway, which depend on root distributions (Notes S1 S.2, 3). Root density is constant within a soil layer, but varies among layers. The model captures hydraulic redistribution simply by the passive flux of water among roots and soil.

The novelty of THORP is how it predicts biomass partitioning (Notes S1 S.8). Our approach is similar to Caldararu *et al.*'s (2020) dynamic nitrogen allocation and approximates Buckley & Roberts' (2006a) dynamic, numerical solution for biomass partitioning within the constraints of the carbon available for allotment. Buckley & Roberts (2006a) solved for the optimal path (referring to the allocation trajectory in either time or tree size) rather than the optimal allometry like traditional optimality models, and we approximate that path (Figs S1 S2). Like previous optimality models, THORP's allocation to a carbon pool ceases when the pool reaches its global optimal (i.e. when the marginal gain is zero, where we maximize gain). Our approach is conceptually similar to maximizing growth, as we have assumed growth rates are a positive, monotonic function of NSC (Notes S1 Eqn S.9.2). Consequently, THORP optimizes net assimilation, leading to elevated NSC and growth. THORP calculates the fraction of carbon allocated during growth to the kth carbon pool, u_k, as

$$u_k \propto \frac{\text{marginal gain}_k}{\text{marginal cost}_k} \qquad \text{Eqn 1(a)}$$

$$\text{Marginal gain}_k = \frac{\partial}{\partial C_k}(a_L(A_n + R_d) - R_m) \qquad \text{Eqn 1(b)}$$

$$\text{Marginal cost}_k = \frac{\partial S_k}{\partial C_k} \qquad \text{Eqn 1(c)}$$

where k may represent leaves, sapwood (stems), or roots in a particular soil layer, the gain is the net canopy photosynthesis minus whole-tree maintenance respiration, $a_L(A_n + R_d) - R_m$ (Bloom *et al.*, 1985), the cost is the senescence rate for the kth carbon pool, S_k (Magnani *et al.*, 2000), A_n is the leaf area-specific net carbon assimilation rate, R_d is the leaf dark respiration, a_L is the total leaf area, and C_k is the size of the kth carbon pool. Allocation fractions are here calculated each day at midday; however, the resulting allometry is the time integral of the product of allocation fraction and growth rate minus the relevant senescence (Notes S1, Eqn S.9.3-5). So while the determination of allocation fractions occurs at daily timescales, allometry better reflects a longer-term mean of the environment. Delays between stimuli and the appearance of allometric responses will be advanced or delayed depending on strength or weakness of growth rates, respectively. See Notes S1 (S.8) for full discussions of our optimization's objective function and dynamic solution.

Marginal gain terms are solved analytically by the following equation which considers the increase in gross carbon assimilation associated with increasing light capture and water use:

$$\text{Marginal gain}_k = (A_n + R_d)\frac{\partial a_L}{\partial C_k} + a_L\wp\frac{\partial I}{\partial C_k} + a_L\lambda\frac{\partial E}{\partial C_k} - \frac{\partial R_m}{\partial C_k}$$
$$\text{Eqn 2}$$

where I is the canopy-averaged light interception, $\wp = \partial A_n/\partial I$ is the marginal light-use efficiency, E is the leaf area-specific transpiration rate, and $\lambda = \partial A_n/\partial E$ is marginal water-use efficiency (Hari *et al.*, 1986). Both $\wp$ and λ represent stress, and their magnitudes drive shifts in allocation towards organs that can alleviate the stress. When water is limiting, λ is large (Mäkelä *et al.*, 1996; Manzoni *et al.*, 2011; Wang *et al.*, 2020), and similarly, when light is limiting, $\wp$ is large. By Eqn 2, large $\wp$ shifts allocation towards shoots which can improve light interception. Similarly, large λ shifts allocation towards sapwood and roots, because their growth can improve the hydraulic efficiency, promote stomatal opening and improve carbon assimilation. As biomass is partitioned to the most limiting organs, the tree adapts to its new environment and becomes less stressed, which causes $\wp$ and/or λ to decline, and allocation can subsequently resume its previous course or shift to alleviate new stresses.

The marginal water-use efficiency, λ, was not explicitly formalized within Sperry *et al.*'s (2017) gain–risk algorithm, but λ may be calculated as a function of leaf water potential, Ψ_L, in the gain–risk framework (Wolf *et al.*, 2016). Following Givnish (1986) and Novick *et al.* (2016a), we interpret λ from the supply function, $E(\Psi_L)$ (Sperry & Love, 2015; Sperry *et al.* 2016), and the gain function, $A_n(\Psi_L)$, as $\lambda = \partial A_n/\partial E = (\partial A_n/\partial\Psi_L)/(\partial E/\partial\Psi_L)$ evaluated at the optimal Ψ_L predicted by the gain–risk algorithm applying a solution by Buckley *et al.* (2017) (Notes S1 Eqn S.6.12). We estimate the marginal light-use efficiency, $\wp$, from A_n's biochemical dependence on electron transport and thus light

capture (Farquhar *et al.*, 1980; Buckley *et al.*, 2002; Notes S1 Eqn S.6.5). Notes S1 (S.8) contains full derivations of the marginal gain and cost terms for each carbon pool and the resulting allocation. Allocation in THORP strives for allometric balance and is the product of environment, physiology, and their feedbacks without recourse to empirical representations of carbon allocation.

THORP assumes instantaneous optimization of allocation (u_k, though not so for biomass, C_k, or growth rate). However, that instantaneity may be disputed by some physiologists, as defining the timescales of optimization remains a major challenge to global change research (Dewar *et al.*, 2009). While some suggest instantaneous optimization for resource competition (King, 1990; Wolf *et al.*, 2016), others suggest the timescales of optimality depend on the predictability and regularity of environmental conditions with no guarantee that plant response remains optimal under novel conditions (Mäkelä *et al.*, 2002; Buckley *et al.*, 2017). Yet, predicating responses to novel conditions is a goal of large-scale modelers. Allocation schemes in most current large-scale models are empirical, which make their allocation predictions limited to the range of observations used for model development. Hence, we apply optimality, albeit an instantaneous one, as an organizing principle to improve existing allocation schemes (Trugman *et al.*, 2019a) and predict responses beyond the range of observations and thus to novel conditions (Franklin *et al.*, 2020).

The THORP model represents key plant mechanisms but ignores others that may serve as secondary drivers of allocation, including delayed xylem refilling or lack of recovery as a result of permanent damage, plant water storage, osmoregulation, and nutrient uptake and partitioning. We would expect the first three processes to affect our results quantitatively, but not qualitatively, and the fourth to affect results under nutrient limitation or when the photosynthetic apparatus changes, which THORP presently cannot predict ($V_{c,max}$ and J_{max} are fixed parameters here; see full discussion of limitations in Notes S1). The model can be adapted to resolve these limitations in the future.

The THORP model was coded in MATLAB. All partial differential equations were solved by explicit finite difference at a 6 h time step, except for the Richards equation which was solved implicitly (Notes S1 S.2). The code is included in Notes S2.

Simulations

We performed 29 simulations to test THORP's predictions of allometry under various stimuli (Table 2; Notes S1 S.10). These experiments simulate the growth of a Scots pine (*Pinus sylvestris*) tree over a 100 yr period in an environment similar to the Poblet nature reserve (Poyatos *et al.*, 2013, 2018; description of site and parameterization in Notes S1 S.10.1) recycling the site's climate from 1948 to 1958 (to stimulate a stable environment) with NOAA re-analysis data (NCEP/NCAR Reanalysis 1; Kalnay *et al.*, 1996), and thus environmental conditions vary both inter- and intra-annually. We parameterized the model with values reported or estimated from the existing literature (Table 3). We note that no parameters were finely tuned to match observations, and by using parameters that are as physically based as possible,

we focus on the model's ability to capture fundamental processes. We test THORP's predictions of size-mediated changes in allometry through the control experiment representing favorable growth conditions and compare with well-established allocation trends. The remaining simulations test THORP's ability to capture trees' sensitivity to water stress, competition for light, atmospheric CO_2 and pruning. We present our results as mass fractions (leaf, LMF; stem, SMF; root, RMF) plotted, after a *c.* 2.6 yr spin-up period for hydrological and physiological conditions to equilibrate, and often against total dry mass to best elucidate the effects of size and the differences between treatments (Poorter & Nagel, 2000; Poorter *et al.*, 2012, 2015), as allometry often better reflects plant size over age (e.g. Brouwer, 1962, 1963; Mencuccini *et al.*, 2005). We test our second hypothesis through our simulations of water stress, for which we report the rooting depth ($Z_{95\%}$ and $Z_{99.5\%}$; Figs 2, 5 (see later), S.6-8) as the depth above which either 95% or 99.5% of root biomass is present. In simulations with groundwater, we report the mean groundwater table depth (Fig. 5 See later).

Results

General behavior of THORP

In the control experiment, the simulated Scots pine grew steadily in height over the 100 yr simulation with rates of height growth slowly declining (Fig. 2a,c), in agreement with well-established observations of asymptotic height growth in time (Mencuccini & Grace, 1996; Magnani *et al.*, 2000). Roots quickly grew down to a depth of 4–5.5 m to equilibrate with the hydrological environment and remained within this range through the remainder of the simulation (Fig. 2a,c), where oscillations reflect seasonality and recycling of meteorological forcing. THORP predicts that LAI generally rises asymptotically towards a value of *c.* 3 (Fig. 2b,d), and like rooting depth, leaf area clearly responds to both intra- and interannual variations in light and water availability.

Leaf and sapwood areas are linearly correlated throughout the control experiment ($a_L = 3243.7 a_{sW}^{1.00}$, $R^2 = 0.996$; Fig. 2e), supporting Shinozaki *et al.*'s (1964) pipe model and agreeing with studies demonstrating that $a_L : a_{sW}$ ratios for Scots pine are weakly correlated with age or size (Poyatos *et al.*, 2007; Hu *et al.*, 2020). THORP captures this linearity through its optimality assumption (Buckley & Roberts, 2006a) without explicitly assuming such behavior for leaf–sapwood partitioning *a priori*. Huber values ($a_{sW} : a_L$) in the control experiment decrease with size (Fig. 2f), agreeing with theoretical arguments (Buckley & Roberts, 2006b) and observations (Rosas *et al.*, 2019). Additionally, THORP predicts xylem water potential profiles that agree well with the real Poblet nature reserve site (Fig. S3). This check on the THORP's representation of plant hydraulics, particularly xylem water potentials, is key to testing THORP's predictions of allometry, as THORP seeks to synchronize hydraulic resistances throughout a tree, and thus xylem water potentials should be reasonably distributed.

Total tree dry mass increases over two orders of magnitude from *c.* 1 kg to *c.* 1600 kg through the control experiment, during which time SMF increased from *c.* 0.36 to *c.* 0.82, RMF

Table 2 Summary of Tree Hydraulics and Optimal Resource Partitioning (THORP) simulations.

Simulation	Description
Control	Free drainage lower boundary condition for soil moisture; no overstory; 410 ppm CO_2 (Supporting Information Notes S1 S.10.1)
Hydrometeorological drought 1	Same as control except 75% precipitation (Notes S1 S.10.2)
Hydrometeorological drought 2	Same as control except 50% precipitation (Notes S1 S.10.2)
Hydrometeorological drought 3–22	Same as control except 50% precipitation and the free drainage condition was replaced with shallow groundwater table (Notes S1 S.10.2); groundwater table was incrementally deepened between simulations from 2 to 80 m; between drought simulations 3 and 12, the groundwater table was consecutively lowered in 2 m increments down to a 20 m depth; between drought simulations 13 and 17, the groundwater table was consecutively lowered in 4 m increments from 24 m down to a 40 m depth; between drought simulations 18 and 22, the groundwater table was consecutively lowered in 8 m increments from 48 m down to a 80 m depth
Above-ground competition	Same as control except with added overstory (Notes S1 S.10.3)
Elevated atmospheric CO_2	Same as control except 600 ppm CO_2 (Notes S1 S.10.3)
Pruning 1	Same as control except shoot biomass reduced by half after *c.* 2.6 yr spin-up[1,2] (Notes S1 S.10.4)
Pruning 2	Same as control except shoot biomass reduced by half after first 30 yr[1,2] (Notes S1 S.10.4)
Pruning 3	Same as control except root biomass reduced by half after *c.* 2.6 yr spin-up[2] (Notes S1 S.10.4)
Pruning 4	Same as control except root biomass reduced by half after first 30 yr s[2] (Notes S1 S.10.4)

[1]Parameters altered to reflect changes in stem hydraulic conductance, wood volume relations, and canopy area assuming that the shoot has been cut in half vertically.
[2]Results reported in Fig. S11.

decreased from *c.* 0.36 to *c.* 0.12, and LMF decreased from *c.* 0.27 to *c.* 0.07 (Fig. 4c See later). These trends agree with previous meta-analyses for woody species, and the magnitudes fall near or within observed ranges (Poorter *et al.*, 2012, 2015; Fig. 3a–c). Root-to-shoot ratios declined with tree size in agreement with a recent meta-analysis (Ledo *et al.*, 2018) and fall well within the ranges synthesized by Poorter *et al.* (2012) (Fig. S4). Davidson (1969) suggested that plants adjust their root-to-shoot ratio to balance nutrient uptake rate and carbon gain, and simple models based on this principle have shown that this ratio must vary with plant size to maximize growth (Reynolds & Thornley, 1982; Mäkelä & Sievanen, 1987; Thornley & Parsons, 2014). THORP reproduces this variation in root-to-shoot ratios solely from hydraulic considerations without considering nutrient limitations, emphasizing the role of plant hydraulics.

Although there are few data on allocation fractions, we compared THORP's predictions of allocation fractions with a recent meta-analysis by Xia *et al.* (2019) (Fig. 4). Xia *et al.* (2019) presented their results in terms of allocation to fine roots and total wood (i.e. stem wood and coarse roots). THORP does not explicitly distinguish between coarse and fine roots, and we estimated these allocation fractions assuming that roots maintained a constant fraction of fine roots equal to 20% of the total root biomass (Oleksyn *et al.*, 1999) and that fine roots had a life span of 0.65 yr (Persson, 1980). Allocation fraction estimates from the control experiment agree with Xia *et al.* (2019), generally falling within their confidence intervals (Fig. 4).

Sensitivity to water stress

Reducing precipitation initially motivated root growth at the expense of shoots (red and gold lines in Figs 3, 4), and roots grew down towards deeper, more stable soil water, growing deepest when precipitation was least and surface soils were driest (Fig. 2a, c) in agreement with functional equilibrium and empirical data of allometry (Poorter & Nagel, 2000; Poorter *et al.*, 2012; Eziz *et al.*, 2017) and rooting depth (Schenk & Jackson, 2002) for woody species. During this initial period, $a_L - a_{sW}$ trends match the control experiment (Fig. 2e–f), while we expected $a_L - a_{sW}$ slopes to flatten (larger Huber values) under water stress from theory (Sperry *et al.*, 2019; Trugman *et al.*, 2019a,b) and observations (Mencuccini & Grace, 1994; DeLucia *et al.*, 2000; Rosas *et al.*, 2019). These theories and observations compounded the effects of both reduced precipitation and reduced atmospheric humidity, while we have focused here exclusively on the impact of precipitation. In light of our findings, we performed two additional experiments identical to the control except with reduced atmospheric humidity (60% and 80% of control relative humidity), which predicted elevated Huber values (Fig. S5), agreeing with theory and observations. THORP's higher sensitivity to atmospheric humidity than soil moisture is consistent with studies demonstrating stomatal conductance's higher sensitivity to humidity than moisture (e.g. Novick *et al.*, 2016b).

However, after *c.* 40 and 60 yr in experiments with 50% and 75% of the control precipitation, these allometric trends changed. Rooting depths shallowed, reaching similar depths as the control experiment (Fig. 2a,c), coinciding with reduced RMF (Fig. 3c,f) and a slight decline in root allocation (Fig. 4c). These results were unexpected and deserve further exploration. These declines in root mass and allocation were mirrored by simultaneous increases in shoot allocation (Figs 3a,b,d–e, 4a–b), which we initially interpreted as a decline in water stress. However, further inspection of other indicators of water stress (heightened water-use efficiency and more negative predawn leaf water potentials; Figs S6b–c,f–g, S7b,c,f,g, S8b,c,f,g) suggested that the trees were more not less stressed after root decline and shallowing. The soil water budget suggests that after roots grew down to their deepest, roots quickly extracted water from the deepest layers where soil water potentials were initially least negative.

Table 3 Parameters in Tree Hydraulics and Optimal Resource Partitioning (THORP) for control simulation and their source.

Symbol	Value	Units	Meaning	Source
Structural metrics				
X_L	0.08	m² mol⁻¹ C	Specific leaf area	Based on Martinez-Vilata et al. (2009) for Scots pine assuming needle dry matter of Scots pine is 50% carbon based on Janssens et al. (1999)
ξ	0.5	–	Empirical form factor ($C_W = \rho_{cS}\xi H D^2$)	From Schiestl-Aalto et al. (2015) for Scots pine. Note that those authors define the form factor differently so we multiply their value of 0.6 by $\pi/4$ to agree with our definition
ρ_{cS}	1.4 × 10⁴	mol C m⁻³	Stem carbon density	From Buckley & Roberts (2006a) who interpreted ξ and ρ_{cS} for lodgepole pine using data from Reid et al. (1974), Ryan (1989) and Litton (2002) and in close agreement with the value used by Schiestl-Aalto et al. (2015) for Scots pine
b_0	64.6	m	Power-law scaling coefficient for height; $H = b_0$ when $D = D_{ref} = 1$ m	Chosen so that diameter, D, corresponding to a height of 12 m, would be 8 cm in agreement with the 12-m-tall Scots pine from the SMEAR II field station (Hyytiälä, southern Finland; Hari & Kulmala, 2005) simulated by Nikinmaa et al. (2013) and other authors (e.g. Schiestl-Aalto et al., 2015)
c_0	0.64	–	Exponent for power-law scaling of height	Regressed from height and diameter data for Scots pine from PROFOUND (Reyer et al., 2019) sites (Hyytiala, Kroof, Peitz and Mencuccini & Grace (1996)
b_1	8.5	m	Power-law scaling coefficient for canopy width; $W = b_1$ when $D = D_{ref} = 1$ m	b_1 and c_1 regressed from relationships between diameter and projected crown area for Scots pine from Pretzsch (2014), assuming that canopies are approximately square
c_1	0.63	–	Exponent for power-law scaling of canopy width	
Respiration, senescence and growth				
$r_R^m{}_{15}$	7.0 × 10⁻⁹	s⁻¹	Carbon pool-specific root maintenance respiration rate at 15°C	Estimated so that total respiration (sum of maintenance and growth respirations) was c. 50% of gross annual photosynthesis, and that c. 50% of total maintenance respiration occurred below ground based on Högberg et al. (2002) for Scots pine
$r_{sW}^m{}_{15}$	2.2 × 10⁻¹²	s⁻¹	Carbon pool-specific sapwood maintenance respiration rate at 15°C	Based on Zha et al. (2004) for Scots pine
f_c	0.28	–	Fraction of carbon spent on construction respiration	From Chung & Barnes (1977) for loblolly pine
τ_L	9.5 × 10⁷	s	Mean life span of leaf pool	From Shiestl-Aalto et al. (2015) For Scots pine
τ_R	9.6 × 10⁷	s	Mean life span of root pool	Estimated assuming that fine roots represent 20% of total root biomass, which is based on means of course- and fine-root biomasses of Scots pine from Oleksyn et al. (1999), that the mean life span of fine roots is 0.65 yr based on Persson (1980), and the mean life span of coarse roots equals that of sapwood
τ_{sW}	1.2 × 10⁹	s	Mean life span of sapwood pool	From Helmisaari & Siltala (1989) for Scots pine
ζ	1 × 10⁻⁷	s⁻¹	Proportionality constant between unloading rate, $G/(1 − f_c)$, and carbon storage pool	Estimated so that nonstructural carbon (NSC) carbon storage when expressed as a concentration (estimated as $C_S(C_L + C_W + C_R)^{-1}$) would be in pseudo-steady-state when integrated over annual timescales from model simulations
Xylem hydraulics				
b_2	9.3 × 10⁻¹	mol H₂O s⁻¹ MPa⁻¹	Power-law scaling coefficient for stem xylem conductance; $k_S = b_2$ when $D = D_{ref} = 1$ m and no heartwood is present	b_2 and c_2 regressed from conductance and diameter data for Scots pine from Mencuccini & Grace (1996); c_2 was fixed such that $k_S \propto H^{1.45}$ for Scots pine when no heartwood is present (Hölttä et al., 2013), and assuming sapwood conductance was 90% of maximum at field conditions (Fig. S13)
c_2	0.93	–	Exponent for power-law scaling of stem conductance	
k_L	1.6 × 10⁻²	mol H₂O m⁻² s⁻¹ MPa⁻¹	Leaf area-specific maximum leaf xylem conductance	Based on Buckley & Roberts (2006a) for loblolly pine
b_L	0.85	MPa	Scaling parameter in Weibull function that describes leaves' vulnerability to embolism	b_L and c_L estimated by fitting Weibull curves to hydraulic conductance data of loblolly pine needles from Domec et al. (2009).
c_L	0.81	–	Exponent in Weibull function that describes leaves' vulnerability to embolism	

Table 3 (Continued)

Symbol	Value	Units	Meaning	Source
b_S	5.32	MPa	Scaling parameter in Weibull function that describes stem's vulnerability to embolism	b_S and c_S estimated by fitting Weibull curves to hydraulic conductance data of Scots pine branches from Torres-Ruiz et al. (2016)
c_S	0.80	–	Exponent in Weibull function that describes stem's vulnerability to embolism	
b_R	1.29	MPa	Scaling parameter in Weibull function that describes roots' conductance loss	b_R and c_R estimated by fitting Weibull curves to below-ground conductance data for Scots pine from Poyatos et al.'s (2018). Poyatos et al.'s (2018) conductance measurements were reported as a function of soil moisture content rather than soil water potential. We developed a soil water retention curve for the Tillar valley soils in the Poblet nature reserve (Prades Mountains, northeast Spain) from their coeval measurements of predawn leaf water potential and volumetric soil water content with which we estimated the soil water potentials for their conductance data (see soil property parameterization below)
c_R	2.65	–	Exponent in Weibull function that describes roots' conductance loss	
$\beta_{R,H}$	3.4×10^3	MPa s mol^{-1} H$_2$O mol C	Proportionality constant between minimum horizontal (intralayer) root hydraulic resistance and C_R^{-1}	$\beta_{R,H}$ and $\beta_{R,V}$ were estimated so that below-ground resistance is 45% of total resistance (Martínez-Vilalta et al., 2007) for Scots pine for a 14-m-tall tree with RMF =0.2 (Poorter et al.,2012), LAI = 0.4 (Poyatos et al., 2013) and Z = 3 m (Fan et al., 2017), when $E = 1.6 \times 10^{-3}$ mol H$_2$O m^{-2} s^{-1}, $\Psi_{pd} = -0.72$, MPa, and Ψ_{md} -1.50 MPa based on Poyatos et al. (2013), assuming root conductance at 80% of maximum for Scots pine based on Lintunen et al. (2019), that 'vertical' and 'horizontal' below-ground resistances are each 50% of the total below-ground resistance, and that more roots within a soil layer are intralayer conductors rather than interlayer conductors ($C_{R,H} = \frac{2}{3}C_{Ri}$; $C_{R, V} = \frac{1}{3}C_R$)
$\beta_{R,V}$	9.4×10^4	MPa mol C s mol^{-1} H$_2$O m^{-2}	Proportionality constant between minimum vertical (interlayer) root hydraulic resistance and $\Delta z^2/C_R$	
Photosynthesis and light capture				
$J_{max,0}$	1.1×10^{-4}	mol C m^{-2} s^{-1}	Maximum rate of electron transport at 17°C	$J_{max,0}$ and $V_{c,max,0}$ are based on values for Scots pine from Kolari et al. (2014).
$V_{c,max,0}$	6.0×10^{-5}	mol C m^{-2} s^{-1}	Maximum carboxylation rate at 17°C	
C'	0.98	–	Curvature parameter for hyperbolic minimum of carboxylation- and electron transport-limited gross photosynthesis rates	From Sperry et al. (2017)
C''	0.90	–	Curvature parameter for hyperbolic minimum of light-limited and maximum electron transport rates	From Sperry et al. (2017)
x	6.9×10^{-7}	mol C J^{-1}	Proportionality constant between J_l and I	Calculated for a quantum yield of 0.3 mol photon (mol e$^-$)$^{-1}$ and an assumed average wavelength of PAR of 550 nm
K_n	0	m^{-1}	Effective light extinction coefficient relative to path length of beams passing through neighboring trees	
κ_L	0.32	–	Effective light extinction coefficient of light passing through target tree	From Mencuccini & Grace (1996) for Scots pine
φ	3.34	–	Ratio of total- to projected-leaf area	From Buckley & Roberts (2006a) for conical pines
Soil properties				
N	15	–	Number of soil layers within soil column	Soil water retention properties (θ_r, $\theta_{s,0}$, n_{VG} and α_{VG}) inferred from measurements of Tillar valley soils in the Poblet nature reserve (Prades Mountains, northeast Spain) by Poyatos et al. (2013, 2018) and Sus et al. (2014) assuming predawn leaf water potentials approximate soil water potentials when corrected for the gravitational pressure gradient
θ_r	0	–	Residual volumetric soil water content	
$\theta_{s,0}$	0.40	–	Saturated volumetric soil water content at ground surface	
n_{VG}	2.70	–	Van Gencuthen (1980) shape parameter ($m_{VG} = 1 - 1/n_{VG}$)	
α_{VG}	1.46	MPa^{-1}	Van Gencuthen (1980) scale parameter	

Table 3 (Continued)

Symbol	Value	Units	Meaning	Source
$K_{soil,sat,0}$	6.0×10^{-7}	m s⁻¹	Saturated hydraulic conductivity at ground surface	From Lampurlanes & Cantero-Martinez (2003) for xerochrept clay loam similar in texture and location to the soils at Tillar valley in the Poblet nature reserve (Prades Mountains, northeast Spain) where Poyatos et al. (2018) measured below-ground conductances
e_n	13.6	m	e-folding depth for exponential decline in porosity with depth	e_n and e_K estimated so that porosity and saturated conductivity were 0.01 and 10^{-11} m s⁻¹, respectively, at a depth of 50 m. Those values were chosen to represent the schist underlying the Tillar valley soils using values from Bear (2007) for unfractured schist. A depth of 50 m was chosen as the depth where the effects of fractures are negligible and is based on nearby electrical resistivity measurements (e.g. Barde-Cabusson et al., 2013; Sendròs et al., 2014) as the depth where resistivity becomes relatively uniform
e_K	3.2	m	e-folding depth for exponential decline in saturated conductivity with depth	

LAI, leaf area index; PAR, photosynthetically active radiation; RMF, root mass fraction.
Parameters were chosen to reflect Scots pine (*Pinus sylvestris*) when available or species of the same genus when parameters could not be estimated for Scots pine. Below-ground hydraulic properties (i.e. those of soil and roots) were estimated to represent the Poblet nature reserve (Prades Mountains, northeast Spain).

However, exponentially reduced soil porosity at depth meant that deeper soil layers were easily dried without infiltration from above or capillary rise from groundwater below in these experiments, leading to severe drying of the entire soil column (Figs S6d,h, S7d,h, S8d,h). Without sufficient access to water at any depth, attempting to minimize below-ground hydraulic resistances became futile (reduced dE/dC_R despite elevated λ in Eqn 2), and the tree sought to reduce hydraulic resistances above ground by allocating to shoots (Figs 3a,b,d,e, 4a,b), although preferentially allocating to stems over leaves, and thereby increased Huber values (Fig. 2f), the latter of which is consistent with theory (Sperry *et al.*, 2019; Trugman *et al.*, 2019a,b) and observations (Mencuccini & Grace, 1994; DeLucia *et al.*, 2000; Rosas *et al.*, 2019). Despite a shift in a_L-a_{sW} trends after soil-column desiccation, LAI was consistently lower than the control throughout the entirety of drier experiments (Fig. 2b,d). Desiccation of the soil column did not occur in other simulations with stable water inputs (i.e. control and experiments with shallow groundwater), in which allometric trends were stable and realistic (Figs 2 S.6d,h, S.9d,h). These results demonstrate the importance of representing realistic soil hydrology, particularly when predicting root traits from dynamic root models.

With the addition of a shallow, 2 m groundwater table under reduced precipitation, roots stayed in close proximity to the groundwater table (Fig. 2a,c), fed by groundwater's capillary rise (Fan *et al.*, 2012, 2017). In similar experiments with gradually deepened groundwater, when groundwater was within several meters of the ground surface, the lower boundaries of both the bulk and the entirety of roots grazed the groundwater table ($Z_{95\%}$ and $Z_{99.5\%}$ in Fig. 5c). As the groundwater deepened (past *c.* 6 m), the lower boundary of the bulk root mass detached from the water table, still deepening with groundwater, although at a shallower slope ($Z_{95\%}$ in Fig. 5c), marking the gradual onset of increasing (though initially small) uptake of recent precipitation to satisfy water needs. Upon further deepening (past *c.* 10 m), the lower boundary of the entire root mass detached from the water table, following the groundwater, but no longer touching ($Z_{99.5\%}$ in Fig. 5c), at which time root water uptake from the capillary fringe diminished. At large depths (past *c.* 30 m deep), groundwater became too deep to sufficiently wet the soil column, the soil column desiccated, and roots switched to a predominantly rain-fed mode of water uptake and shallowed to near control rooting depths (similar to the previous experiments without groundwater) ($Z_{95\%}$ in Fig. 5a–c). Nonetheless, even at these great depths, the lower boundary of the entire root mass continues to slightly deepen with groundwater ($Z_{99.5\%}$ in Fig. 5c) despite the shallowing bulk root mass ($Z_{95\%}$). Although rooting depths varied by more than an order of magnitude, RMF was relatively stable and within realistic bounds (Fig. 5e). Generally, RMF increased as the groundwater deepened, consistent with functional equilibrium. However, when groundwater was deeper than *c.* 30 m, RMF eventually declined despite increased water stress in experiments as a result of desiccation of the soil column, as in experiments with reduced precipitation and no groundwater.

Groundwater's presence alleviated the water stress associated with reduced precipitation (increased water-use efficiency and less
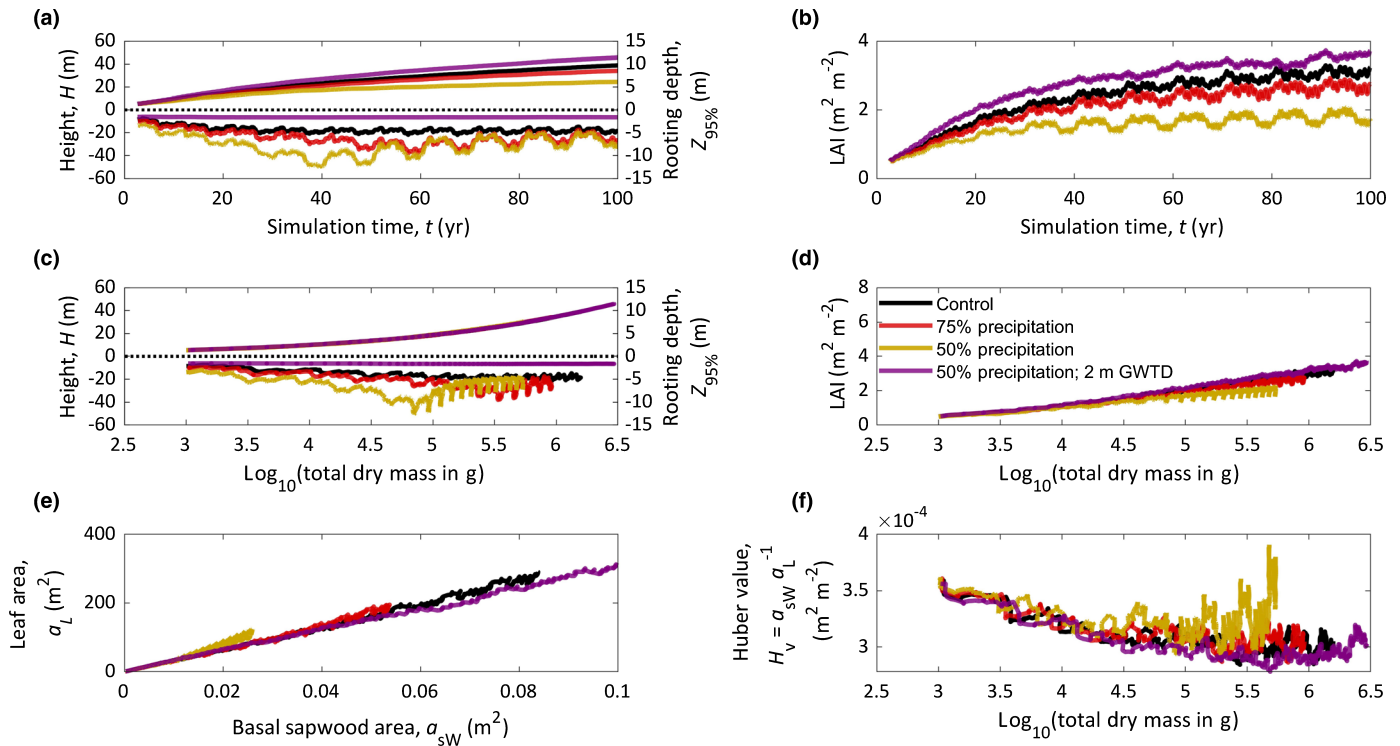
Fig. 2 Time series of the Tree Hydraulics and Optimal Resource Partitioning (THORP) model predictions of tree dimensions for 100-yr control experiment (black line) and experiments with reduced precipitation (75% and 50% of control; red and yellow lines, respectively). An additional experiment, also with 50% precipitation of the control, was simulated with the free-drainage lower boundary condition for soil moisture replaced by a shallow, 2-m-deep groundwater table (purple line). Progressions of height and rooting depth (defined as the depth to a 95% cumulative root fraction) (a, c) and leaf area index ($a_L \varphi^{-1} W^{-2}$) (b, d) vs time (a, b) and size, expressed as total dry mass (c, d). (e) Relationship between basal sapwood and total leaf areas. (f) Huber value (sapwood : leaf area ratio, $a_{sW} : a_L$) vs tree size. In (c), height curves overlap for all experiments. All values were averaged over monthly time steps to clarify trends.

negative predawn leaf water potentials; Fig. S9b,c,f,g), enabling faster growth, enhanced LAI, LMF, SMF and allocation to shoots, and reduced RMF and allocation to roots compared with experiments with reduced precipitation and even the control (Figs 2a,b,d,e–4). Unlike the solely rain-fed simulations, the experiment with shallow, 2-m-deep groundwater shows reduced response in rooting depth, LAI, and Huber values to the recycling of forcing data (Fig. 2), because groundwater provides a stable water source regardless of meteorological variability. This stabilizing influence diminished as groundwater deepened and trees increasingly relied on precipitation (Fig. 5a,b and confidence intervals in Fig. 5c). These results demonstrate rooting depth's sensitivity to soil hydrology and support our second hypothesis.

Deep roots are often defined as deeper than 2 m (e.g. Schenk & Jackson, 2005). Similarly, vegetation models traditionally distribute their root mass above 2 m even when root mass exponentially declines with depth (e.g. CLM v.4.0-5.0; Oleson *et al.*, 2010, 2013; Lawrence *et al.*, 2019; Shao *et al.*, 2019), despite the fact that observed maximum rooting depths are often far deeper (e.g. Canadell *et al.*, 1996; Schenk & Jackson, 2002; Fan *et al.*, 2017). To emphasize the importance of deep roots and groundwater, we show the fraction of midday transpiration sourced from below 2 m (Fig. 5d). In simulations with roots deeper than 2 m, at least *c.* 10% of transpiration was sourced by deep roots, and more than three times as much (*c.* 35%) was taken up at depth

when groundwater was shallower than *c.* 30 m, when roots could directly access the capillary fringe.

Above-ground competition and elevated atmospheric CO_2

The addition of an overstory caused a rapid shift in allometry towards stem growth to improve the target tree's light interception (green line in Fig. 6a). SMF quickly spiked *c.* 40% relative to the control experiment (Fig. 6e), to reach a height of *c.* 7.5 m, after which point SMF remained near constant at *c.* 80% until reaching the height of the upper canopy (30 m) (Fig. 6b). As SMF initially rose, RMF and LMF dropped *c.* 25% and *c.* 15%, respectively (Fig. 6d,f). The differences in SMF and RMF between the experiment with the overstory and the control experiment became smaller as the target tree grew taller and as light interception improved. Stem growth was prioritized to increase height, as the tree was most limited by the vertical attenuation of light through the upper canopy, consistent with common knowledge that light competition drives trees to grow taller (Onoda *et al.*, 2014). The increase in SMF and decrease in RMF agree with both the functional equilibrium hypothesis and syntheses of observed allometric responses to low irradiance (Poorter & Nagel, 2000; Poorter *et al.*, 2012; Fig. 1). However, the reduced LMF contrasts with functional equilibrium and the same syntheses on observed allometry on the effects of low irradiance. Other
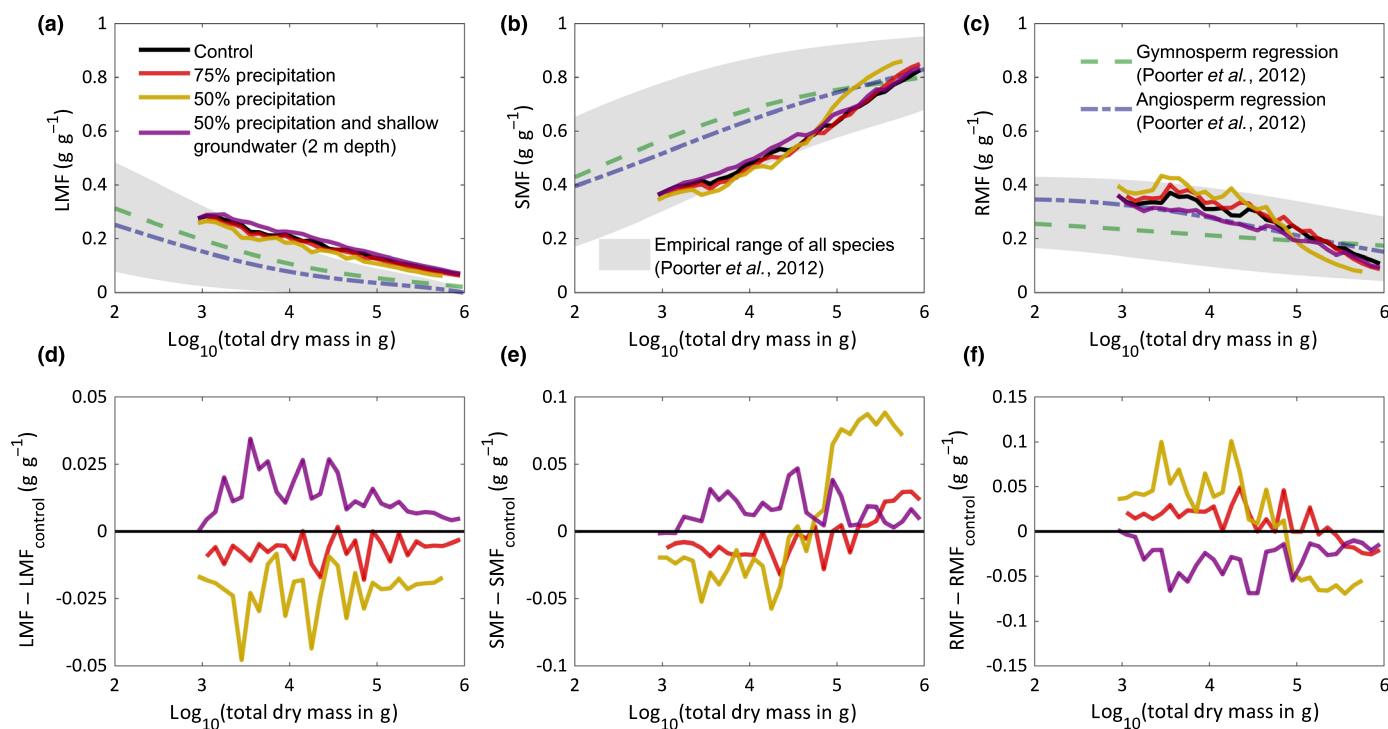
Fig. 3 Tree Hydraulics and Optimal Resource Partitioning (THORP) model predictions of mass fractions for 100-yr control experiment (black line) and experiments with reduced precipitation (75% and 50% of control; red and yellow lines, respectively). An additional experiment, also with 50% precipitation of the control, was simulated with the free-drainage lower boundary condition for soil moisture replaced by a shallow, 2-m-deep groundwater table (purple line). Mass fraction of leaves (LMF), stems (SMF) and roots (RMF) (a–c) and their differences relative to the control experiment (d–f) vs size, expressed as total dry mass. THORP's predictions were binned into logarithmically spaced biomass pools ([$10^{3.0}$, $10^{3.1}$], [$10^{3.1}$, $10^{3.2}$], [$10^{3.2}$, $10^{3.3}$], etc.) and averaged to clarify trends. To compare THORP's predictions with observations, we also plotted the size-dependent trends in LMF, SMF and RMF as synthesized by Poorter *et al*. (2012; extracted from their Figs 2; Supporting Information Fig. S2). Poorter *et al*. (2012) derived average trends separately for woody angiosperms (blue double-dashed line) and gymnosperms (green dashed line). Gray, shaded areas represent confidence bounds for each mass fraction estimated by Poorter *et al*.'s (2012) synthesis. Poorter *et al*. (2012) did not report the uncertainty of their statistical trends; however, we estimated these bounds by the method of variance using values extracted from their Fig. S2. We assumed that the SD for the log_{10} leaf and stem dry mass (in g): were independent of the magnitude of root dry mass; could be approximated by one-quarter of the range of the same values after removing the linear size trend (i.e. that their ranges were *c*. 95% of their theoretical distributions and that the distributions of log_{10} of organ-specific dry masses were normally distributed); and were equal to *c*. 0.37 and *c*. 0.39, respectively, based on Poorter *et al*.'s (2012) Fig. S2.

analyses by Poorter *et al*. (2012) demonstrated that plants grown at high density have, on average, increased SMF and slightly reduced LMF and RMF which was attributed to light competition in closed canopies where gaining stem height is most crucial and which agrees better with our results. LMF reduced in THORP partially because of increased priority for stem growth, but also because of a decrease in priority for leaf growth. The addition of the overstory reduced the marginal gain for the leaf carbon pool by *c*. half relative to the control. It is not surprising that THORP predicts decreased leaf biomass under lower light conditions, as previous optimality approaches predict LAI that asymptotically increases with insolation (Caldararu *et al*., 2012, 2014). We believe that representing the plasticity in traits, especially specific leaf area and maximum carboxylation rate (X_L and $V_{c,max,0}$ in Table 3), would improve THORP's predictions of leaf allocation under low light, as they vary between upper and lower canopies (Meir *et al*. 2002).

Elevated atmospheric CO_2 concentrations (eCO$_2$; 600 ppm) induced an increase in LMF and a decrease in RMF relative to the control that gradually declined with time (or size) (orange lines in Fig. 6d,f). The small increase in LMF that persisted by the end of

the experiment (< 1%) can be explained by elevated carbon assimilation rates under eCO$_2$ (A_n directly spurs leaf allocation through Eqn 2; Fig. S10b). eCO$_2$ is expected to cause stomata closure (Morison, 1987) and thus increased λ (Katul *et al*., 2010), from which we expected allocation to shift towards hydraulic structures like roots and stems through Eqn 2. Although THORP predicted increased λ under eCO$_2$ (expressed by proxy in Fig. S10a), RMF initially decreased as much as *c*. 7% relative to the control, and only by the end was RMF under eCO$_2$ slightly larger than the control (*c*. 1%). Further exploration of the experienced water stress and soil moisture (Fig. S10) suggests that the initial large increase in LMF and large decrease in RMF were not directly induced by eCO$_2$, but rather by improved water status indirectly caused by eCO$_2$. Stomatal closure under eCO$_2$ reduced transpiration and root water uptake and thus maintained a wetter soil column (Fig. S10d). This excess soil moisture enabled the tree initially to behave as if it were less water-stressed (Fig. S10a–c), shifting allocation towards leaves and away from roots as in experiments that tested the sensitivity to water stress (Figs 2–4). By the end of the experiment, only the direct effects of eCO$_2$ are apparent, when the differences in mass fractions between the eCO$_2$ experiment and the
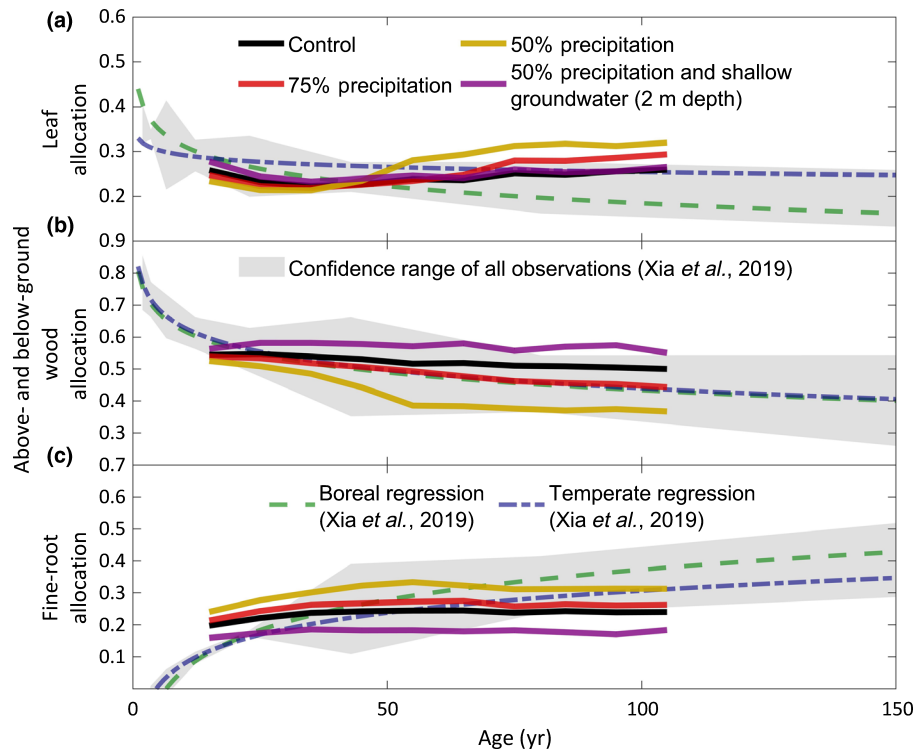
Fig. 4 Tree Hydraulics and Optimal Resource Partitioning (THORP) model predictions of allocation fractions for 100 yr control experiment (black line) and experiments with reduced precipitation (75% and 50% of control; red and yellow lines, respectively). An additional experiment, also with 50% precipitation of the control, was simulated with the free-drainage lower boundary condition for soil moisture replaced by a shallow, 2-m-deep groundwater table (purple line). (a–c) Allocation fractions to leaves (a), wood (b) and fine roots (c). Note that THORP does not explicitly distinguish between coarse and fine roots, and we estimated these allocation fractions from model results assuming that roots maintained a constant fraction of fine roots equal to 20% of the total root biomass (Oleksyn *et al.*, 1999) and that fine roots had a life span of 0.65 yr (Persson, 1980). We further assumed that the initial sapling was 5 yr old. Values are averaged over the period of the forcing data (10 yr) to clarify trends. To compare THORP's predictions to observations, we also plotted the age-dependent trends in allocation as synthesized by Xia *et al*. (2019; adapted from their Fig. 3) for boreal (green dashed lines) and temperate (blue double-dashed lines) forest. Gray, shaded areas represent *c.* 99% confidence intervals of Xia *et al.*'s (2019) supplementary data that we estimated by assuming allocation fractions were normally distributed.

control are small (absolute value ≤ 1.5%). This behavior agrees well with meta-analyses showing plants, on average, negligibly change their allometry in response to eCO_2 when nutrients are not limiting (Stulen & Hertog, 1993; Poorter & Nagel, 2000; Poorter *et al.*, 2012), but not with functional equilibrium, which holds CO_2 as an above-ground resource and would expect an increase in root allocation.

Discussion

We present the THORP model, which predicts the dynamic carbon allocation that maximizes assimilation. Biomass partitioning in THORP is solved by an analytical solution which is computationally efficient without recourse to parameters that explicitly control allocation, and its general framework in a simplified form may be appropriate for integration into large-scale vegetation modeling. We demonstrate that THORP predicts the biomass partitioning of trees as a function of size and in response to water limitations, eCO_2 (without nutrient limitation) and pruning (Poorter & Nagel, 2000; Poorter *et al.*, 2012, 2015; Eziz *et al.*, 2017; Xia *et al.*, 2019), and agrees with much of functional equilibrium (Brouwer, 1962, 1963) for the same effects (size, water,

CO_2, pruning) (Figs 2–4). THORP captures the coordination of leaf and sapwood areas as a function of size (Buckley & Roberts, 2006b) and under water stress (Sperry *et al.*, 2019; Trugman *et al.*, 2019a,b) (Figs 2e–f S10) and recovery responses after allometric changes (Brouwer, 1962; Fig. S11). These results supports our first hypothesis that hydraulic demands are key drivers of tree allocation.

An increase in root production and decline in LAI is often observed in free air CO_2 enrichment (FACE) experiments, and these changes are often interpreted as a response to increase nutrient uptake to enable faster growth (Norby *et al.*, 2006; Finzi *et al.*, 2007; Franklin, 2007; Pritchard *et al.*, 2008; Franklin *et al.*, 2009, 2012; Jackson *et al.*, 2009; Iversen, 2010). THORP neither describes nutrient acquisition nor reproduces these FACE observations under eCO_2 (Fig. 6). While our other experiments demonstrated that much of plant allometry could be predicted from hydraulic considerations (Figs 2–4), these results demonstrate that nutrient status cannot be fully ignored. Likewise, THORP correctly predicts trends in stem and root partitioning under competition for light, but like previous optimality models (Caldararu *et al.*, 2012, 2014), THORP predicts smaller leaf areas under low light for a given tree size (Fig. 6a,d). Traits like
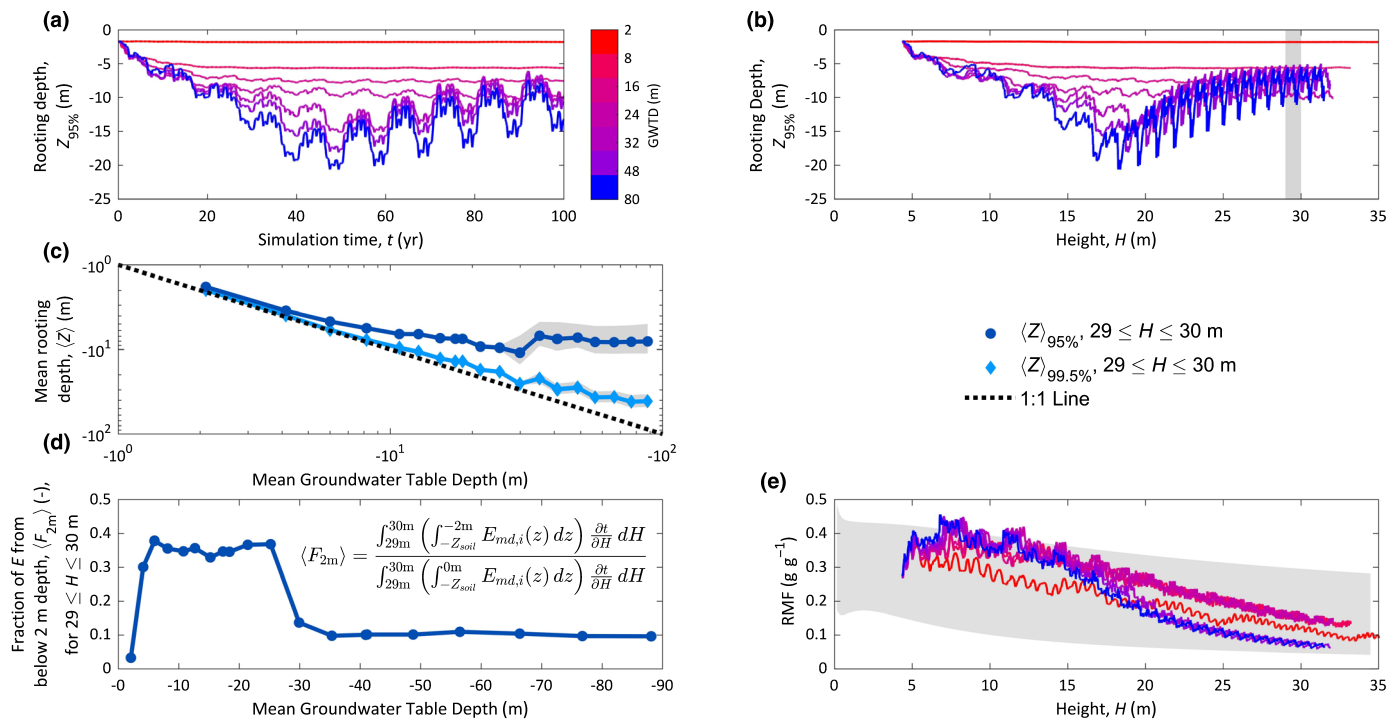
Fig. 5 Tree Hydraulics and Optimal Resource Partitioning (THORP) model predictions of rooting depth, profiles, and water uptake from experiments with reduced precipitation (50% of control) and various groundwater depths (red-to-blue for shallow-to-deep groundwater as shown in the color bar in (a)). Rooting depths, $Z_{95\%}$ (a–c) and $Z_{99.5\%}$ (c) (defined as the depths to 95% and 99.5% cumulative root fractions, respectively) vs time (a), height (b) and mean simulated groundwater table depth. Gray, shaded areas in (b) reflect heights between 29 and 30 m. In (c) and (d), values are averaged temporally for periods when trees fell into a standardized height class between 29 and 30 m, corresponding to the gray, shaded area in (b). Gray, shaded areas in (c) represent the 95% confidence intervals for rooting depths within the 29–30 m height class. The outer integrals in both the numerator and denominator in the equation in (d) represent the temporal average, although the bounds of integration are written in terms of height (note the substitutional conversions through $\partial t/\partial H$ terms). (d) Fraction of total time-integrated midday root-water uptake, $E_{md,i}$ (analogous to Notes S1 Eqn S.2.2, although written continuously with depth rather than in discrete notation), sourced from below 2 m deep, $\langle F_{2m} \rangle$. (e) Root mass fraction (RMF). Gray, shaded area in (e) represents confidence bounds for RMF for Poorter *et al.*'s (2012) synthesis (same as Fig. 3c) for trees following Poorter *et al.*'s (2012) mean stem mass fraction (SMF) size trend, applying parameters in Table 3 to convert between stem biomass and height, assuming wood is 50% carbon by mass. Note that these bounds underestimate the range in root mass fraction (RMF), as all trees may not follow the mean SMF size trend.

specific leaf area and maximum carboxylation rate are constant in THORP, and representing their plasticity may correct this limitation. These traits are linked to trees' nutrient budget (Field & Mooney, 1986; Evans, 1989; Meir *et al.* 2002), further suggesting that nutrient status must be considered when simulating vegetation responses to stimuli that alter photosynthetic efficiency ($V_{c,max}$ and J_{max}).

Root profiles in rain-fed experiments were sensitive to atmospheric conditions which directed root allocation through the resulting soil moisture distributions. When shallow groundwater was introduced, soil moisture stabilized and roots deepened, following the groundwater table (Naumburg *et al.*, 2005; Christina *et al*, 2017; Fan *et al.*, 2017) regardless of fluctuating atmospheric conditions (Fig. 5). Roots grew to their deepest when the groundwater table was *c.* 30 m deep. At deeper groundwater depths, the costs of deep roots exceeded the benefits of accessible groundwater, and roots shallowed and attuned to precipitation regimes, behaving as in the rain-fed experiments independent of groundwater (Fan *et al.*, 2017). These results support our second hypothesis that root allocation is attuned to soil hydrology. Through this attunement, moisture derived from deep soils supported a significant fraction of root water uptake regardless of

depth (Fig. 5) and buffered the effects of hydrometeorological drought on rooting depth, biomass portioning and leaf : sapwood area ratios (Fig. 2).

Our results suggest that application of THORP and similar models that predict rooting distributions from soil moisture profiles (Table 1) require accurate modeling of soil hydrology. Roots grew down to the groundwater table when present regardless of depth if growing under insufficient precipitation (Fig. 5), and thus the groundwater table may be an important ecophysiological boundary, the role of which should be further investigated (Dawson *et al.*, 2020). However, few large-scale land models explicitly simulate groundwater processes (Clark *et al.*, 2015; Fan *et al.*, 2019). This lack of groundwater suggests that large-scale models may overestimate the water stress experienced by plants for large portions of the land surface. Fan *et al.* (2013) suggested that up to a third of the land surface has groundwater shallow enough to interact with most plants either directly or indirectly though the capillary fringe. In these regions, groundwater reduces mortality (Tai *et al.*, 2018; Love *et al.*, 2019; Mackay *et al.*, 2020; McLaughlin *et al.*, 2020), improves productivity (Roebroek *et al.*, 2020), and contributes to biodiversity (McLaughlin *et al.*, 2017). Our results demonstrate that through
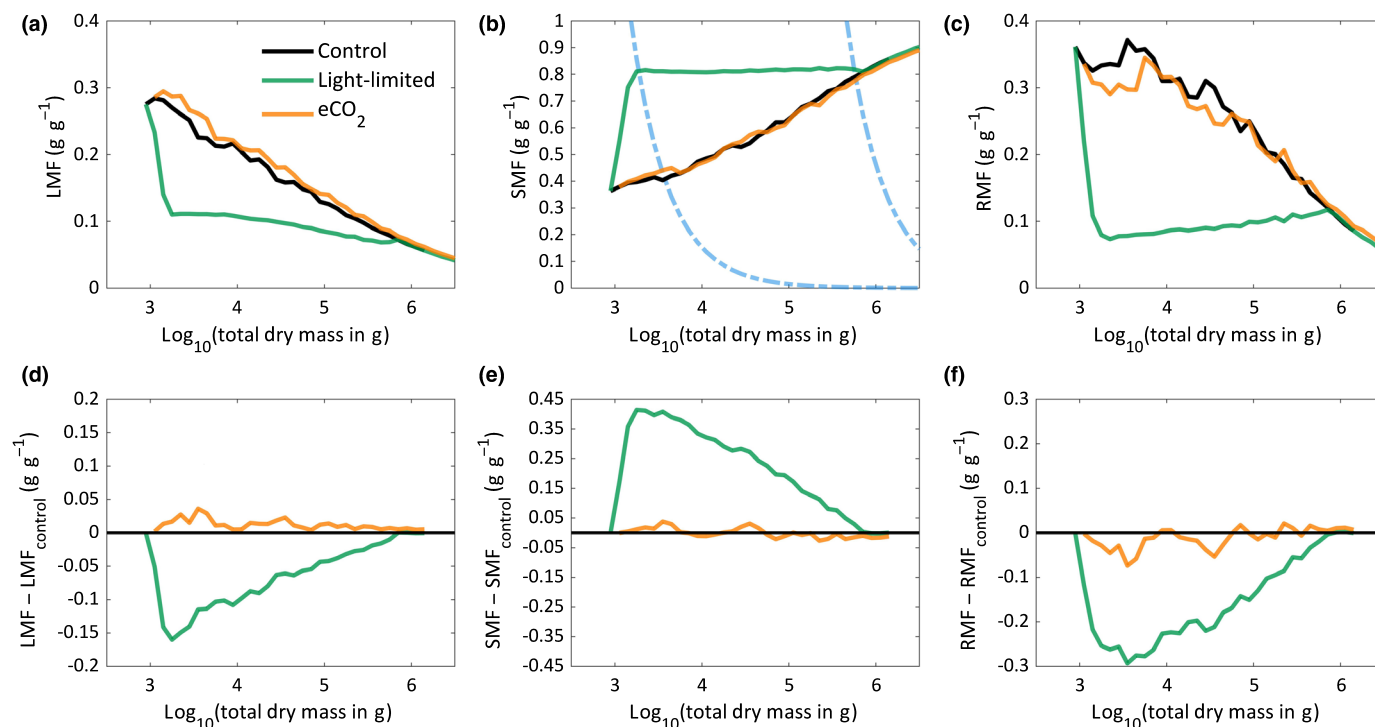
Fig. 6 Tree Hydraulics and Optimal Resource Partitioning (THORP) model predictions for experiments under an elevated atmospheric CO_2 concentration (eCO$_2$; 600 pm) and with a 30-m-high upper canopy to reflect competition for light. (a–f) Mass fraction of leaves (LMF), stems (SMF) and roots (RMF) (a–c) and their differences relative to the control experiment (d–f) vs size, expressed as total dry mass. Two blue double-dashed lines in (b) represent SMF required for heights equal to 7.5 and 30 m.

deep roots, groundwater need not be as shallow as assumed by Fan *et al.* (2013) to influence vegetation. When precipitation was insufficient, roots deepened, and tree allometry and water use were influenced by groundwater as deep as *c.* 30 m (Fig. 5), thereby potentially extending the portion of the global land surface where groundwater may influence vegetation. Furthermore, without groundwater tables to constrain where roots grow, the application of THORP or similar root models (e.g. Schymanski *et al.*, 2008, 2009; Sivandran & Bras, 2013; Fan *et al.*, 2017) to large-scale models will over-predict rooting depth over much of the land surface. Thus, deep roots may enable strong feedbacks between hydrology and vegetation over much of the continents, and understanding and predicting these feedbacks further necessitates representing hydrological realism in large-scale land in tandem with improving vegetation modeling schemes.

Author contributions

AP, CRCM and YF, designed the model. AP, YW and MDV coded the model. AP, ATT, WRLA and YF designed the simulation experiments. AP ran the model and analyzed simulated data. AP led the writing. All authors contributed to data interpretation, discussion and the final version of the manuscript.

ORCID

William R. L. Anderegg (iD) https://orcid.org/0000-0001-6551-3331
Ying Fan (iD) https://orcid.org/0000-0002-0024-7965
Aaron Potkay (iD) https://orcid.org/0000-0003-3101-2701
Anna T. Trugman (iD) https://orcid.org/0000-0002-7903-9711
Martin D. Venturas (iD) https://orcid.org/0000-0001-5972-9064
Yujie Wang (iD) https://orcid.org/0000-0002-3729-2743

References

Aber JD, Melillo JM, Nadelhoffer KJ, McClaugherty CA, Pastor J. 1985. Fine root turnover in forest ecosystems in relation to quantity and form of nitrogen availability: A comparison of two methods. *Oecologia* **66**: 317–321.

Alder NN, Sperry JS, Pockman WT. 1996. Root and stem xylem embolism, stomatal conductance, and leaf turgor in *Acer grandidentatum* populations along a soil moisture gradient. *Oecologia* **105**: 293–301.

Anten NP, During HJ. 2011. Is analysing the nitrogen use at the plant canopy level a matter of choosing the right optimization criterion? *Oecologia* **167**: 293–303.

Arora VK, Boer GJ. 2005. A parameterization of leaf phenology for the terrestrial ecosystem component of climate models. *Global Change Biology* **11**: 39–59.

Ballantyne AP, Andres R, Houghton R, Stocker BD, Wanninkhof R, Anderegg W, Cooper LA, DeGrandpre M, Tans PP, Miller JB *et al.* 2015. Audit of the global carbon budget: estimate errors and their impact on uptake uncertainty. *Biogeosciences* **12**: 2565–2584.

Barde-Cabusson S, Bolós X, Pedrazzi D, Lovera R, Serra G, Martí J, Casas A. 2013. Electrical resistivity tomography revealing the internal structure of monogenetic volcanoes. *Geophysical Research Letters* 40: 2544–2549.

Barigah TS, Bonhomme M, Lopez D, Traore A, Douris M, Venisse J-S, Cochard H, Badel E. 2013. Modulation of bud survival in *Populus nigra* sprouts in response to water stress-induced embolism. *Tree Physiology* 33: 261–274.

Bear J. 2007. *Hydraulics of groundwater*. Mineola, NY, USA: Dover Publications.

Beer C, Reichstein M, Tomelleri E, Ciais P, Jung M, Carvalhais N, Rodenbeck C, Arain MA, Baldocchi D, Bonan GB *et al*. 2010. Terrestrial gross carbon dioxide uptake: global distribution and covariation with climate. *Science* 329: 834–838.

Beven KJ, Kirkby MJ. 1979. A physically based, variable contributing area model of basin hydrology. *Hydrological Sciences Bulletin* 24: 43–69.

Bloom AJ, Chapin FS III, Mooney HA. 1985. Resource limitation in plants-an economic analogy. *Annual Review of Ecology and Systematics* 16: 363–392.

Bonan GB. 2008. Forests and climate change: forcings, feedbacks, and the climate benefits of forests. *Science* 320: 1444–1449.

Bonan G. 2015. *Ecological climatology: concepts and applications*. Cambridge, UK: Cambridge University Press.

Brouwer R. 1962. Nutritive influences on the distribution of dry matter in the plant. *Netherlands Journal of Agricultural Sciences* 10: 361–376.

Brouwer R. 1963. Some aspects of the equilibrium between overground and underground plant parts. *Jaarboek van het Instituut voor Biologisch en Scheikundig onderzoek aan Landbouwgewassen* 1963: 31–39.

Buckley TN, Miller JM, Farquhar GD. 2002. The mathematics of linked optimisation for water and nitrogen use in a canopy. *Silva Fennica* 36: 639–669.

Buckley TN, Roberts DW. 2006a. DESPOT, a process-based tree growth model that allocates carbon to maximize carbon gain. *Tree Physiology* 26: 129–144.

Buckley TN, Roberts DW. 2006b. How should leaf area, sapwood area and stomatal conductance vary with tree height to maximize growth? *Tree Physiology* 26: 145–157.

Buckley TN, Sack L, Farquhar GD. 2017. Optimal plant water economy. *Plant, Cell & Environment* 40: 881–896.

Caldararu S, Palmer PI, Purves DW. 2012. Inferring Amazon leaf demography from satellite observations of leaf area index. *Biogeosciences* 9: 1389–1404.

Caldararu S, Purves DW, Palmer PI. 2014. Phenology as a strategy for carbon optimality: a global model. *Biogeosciences* 11: 763–778.

Caldararu S, Thum T, Yu L, Zaehle S. 2020. Whole-plant optimality predicts changes in leaf nitrogen under variable CO_2 and nutrient availability. *New Phytologist* 225: 2331–2346.

Canadell J, Jackson RB, Ehleringer JB, Mooney HA, Sala OE, Schulze ED. 1996. Maximum rooting depth of vegetation types at the global scale. *Oecologia* 108: 583–595.

Carter JL, White DA. 2009. Plasticity in the Huber value contributes to homeostasis in leaf water relations of a mallee Eucalypt with variation to groundwater depth. *Tree Physiology* 29: 1407–1418.

Chen X, Eamus D, Hutley LB. 2004. Seasonal patterns of fine-root productivity and turnover in a tropical savanna of northern Australia. *Journal of Tropical Ecology* 20: 221–224.

Christina M, Nouvellon Y, Laclau J-P, Stape JL, Bouillet J-P, Lambais GR, Lambais GR, Maire G. 2017. Importance of deep water uptake in tropical eucalypt forest. *Functional Ecology* 31: 509–519.

Christoffersen BO, Gloor M, Fauset S, Fyllas NM, Galbraith DR, Baker TR, Kruijt B, Rowland L, Fisher RA, Binks OJ *et al*. 2016. Linking hydraulic traits to tropical forest function in a size-structured and trait-driven model (TFS v.1-Hydro). *Geoscientific Model Development* 9: 4227–4255.

Chung HH, Barnes RL. 1977. Photosynthate allocation in *Pinus taeda taeda*. I. Substrate requirements for synthesis of shoot biomass. *Canadian Journal of Forest Research* 7: 106–111.

Clark MP, Fan Y, Lawrence DM, Adam JC, Bolster D, Gochis DJ, Hooper RP, Kumar M, Leung LR, Mackay DS. 2015. Improving the representation of hydrologic processes in earth system models. *Water Resources Research* 51: 5929–5956.

Collins DBG, Bras RL. 2007. Plant rooting strategies in water-limited ecosystems. *Water Resources Research* 43: W06407.

Davidson RL. 1969. Effect of root/leaf temperature differentials on root/shoot ratios in some pasture grasses and clover. *Annals of Botany* 33: 561–569.

Dawson TE, Hahm WJ, Crutchfield-Peters K. 2020. Digging deeper: what the critical zone perspective adds to the study of plant ecophysiology. *New Phytologist* 226: 666–671.

De Kauwe Martin G, Medlyn BE, Zaehle S, Walker Anthony P, Dietze Michael C, Wang Y-P, Luo Y, Jain Atul K, El-Masri B, Hickler T *et al*. 2014. Where does the carbon go? A model–data intercomparison of vegetation carbon allocation and turnover processes at two temperate forest free-air CO_2 enrichment sites. *New Phytologist* 203: 883–899.

Delucia EH, Maherali H, Carey EV. 2000. Climate-driven changes in biomass allocation in pines. *Global Change Biology* 6: 587–593.

Dewar RC, Franklin O, Mäkelä A, McMurtrie RE, Valentine HT. 2009. Optimal function explains forest responses to global change. *BioScience* 59: 127–139.

Domec JC, Palmroth S, Ward E, Maier CA, Therezien M, Oren R. 2009. Acclimation of leaf hydraulic conductance and stomatal conductance of *Pinus taeda* (loblolly pine) to long-term growth in elevated CO_2 (free-air CO_2 enrichment) and N-fertilization. *Plant, Cell & Environment* 32: 1500–1512.

Drewniak B, Gonzalez-Meler MA. 2017. Earth system model needs for including the interactive representation of nitrogen deposition and drought effects on forested ecosystems. *Forests* 8: 267.

Dybzinski R, Farrior C, Wolf A, Reich PB, Pacala SW. 2011. Evolutionarily stable strategy carbon allocation to foliage, wood, and fine roots in trees competing for light and nitrogen: an analytically tractable, individual-based model and quantitative comparisons to data. *American Naturalist* 177: 153–166.

Dybzinski R, Farrior CE, Pacala SW. 2015. Increased forest carbon storage with increased atmospheric CO_2 despite nitrogen limitation: A game-theoretic allocation model for trees in competition for nitrogen and light. *Global Change Biology* 21: 1182–1196.

Eller CB, Rowland L, Mencuccini M, Rosas T, Williams K, Harper A, Medlyn BE, Wagner Y, Klein T, Teodoro GS *et al*. 2020. Stomatal optimization based on xylem hydraulics (SOX) improves land surface model simulation of vegetation responses to climate. *New Phytologist* 226: 1622–1637.

Evans JR. 1989. Photosynthesis and nitrogen relationships in leaves of C_3 plants. *Oecologia* 78: 9–19.

Eziz A, Yan Z, Tian D, Han W, Tang Z, Fang J. 2017. Drought effect on plant biomass allocation: A meta-analysis. *Ecology and Evolution* 7: 11002–11010.

Fan Y, Clark M, Lawrence DM, Swenson S, Band LE, Brantley SL, Brooks PD, Dietrich WE, Flores A, Grant G *et al*. 2019. Hillslope hydrology in global change research and earth system modeling. *Water Resources Research* 55: 1737–1772.

Fan Y, Li H, Miguez-Macho G. 2013. Global patterns of groundwater table depth. *Science* 339: 940–943.

Fan Y, Miguez-Macho G, Jobbágy EG, Jackson RB, Otero-Casal C. 2017. Hydrologic regulation of plant rooting depth. *Proceedings of the National Academy of Sciences, USA* 114: 10572–10577.

Farquhar GD, von Caemmerer S, Berry JA. 1980. A biochemical model of photosynthetic CO_2 assimilation in leaves of C_3 species. *Planta* 149: 78–90.

Farrior CE, Dybzinski R, Levin SA, Pacala SW. 2013. Competition for water and light in closed-canopy forests: a tractable model of carbon allocation with implications for carbon sinks. *American Naturalist* 181: 314–330.

Fatichi S, Leuzinger S, Körner C. 2014. Moving beyond photosynthesis: from carbon source to sink-driven vegetation modeling. *New Phytologist* 201: 1086–1095.

Field CH, Mooney HA. 1986. Photosynthesis–nitrogen relationship in wild plants. In: *On the economy of plant form and function: proceedings of the Sixth Maria Moors Cabot symposium, evolutionary constraints on primary productivity, adaptive patterns of energy capture in plants, Harvard Forest, August 1983*. Cambridge, UK: Cambridge University Press, 1986.

Finzi AC, Norby RJ, Calfapietra C, Gallet-Budynek A, Gielen B, Holmes WE, Hoosbeek MR, Iversen CM, Jackson RB, Kubiske ME *et al*. 2007. Increases in nitrogen uptake rather than nitrogen-use efficiency support higher rates of temperate forest productivity under elevated CO_2. *Proceedings of the National Academy of Sciences, USA* 104: 14014–14019.

Franklin O. 2007. Optimal nitrogen allocation controls tree responses to elevated CO_2. *New Phytologist* 174: 811–822.

Franklin O, Harrison SP, Dewar R, Farrior CE, Brännström Å, Dieckmann U, Pietsch S, Falster D, Cramer W, Loreau M *et al.* 2020. Organizing principles for vegetation dynamics. *Nature Plants* 6: 444–453.

Franklin O, Johansson J, Dewar RC, Dieckmann U, McMurtrie RE, Brännström Å, Dybzinski R. 2012. Modeling carbon allocation in trees: a search for principles. *Tree Physiology* 32: 648–666.

Franklin O, McMurtrie RE, Iversen CM, Crous KY, Finzi AC, Tissue DT, Ellsworth DS, Oren R, Norby RJ. 2009. Forest fine-root production and nitrogen use under elevated CO_2: contrasting responses in evergreen and deciduous trees explained by a common principle. *Global Change Biology* 15: 132–144.

van Genuchten MT. 1980. A closed-form equation for predicting the hydraulic conductivity of unsaturated soils 1. *Soil Science Society of America journal* 44: 892–898.

Givnish TJ. 1986. Optimal stomatal conductance, allocation of energy between leaves and roots, and the marginal cost of transpiration. In: Givnish TJ, ed. *On the economy of plant form and function: proceedings of the Sixth Maria Moors Cabot symposium, evolutionary constraints on primary productivity, adaptive patterns of energy capture in plants, Harvard Forest, August 1983*. Cambridge, UK: Cambridge University Press, 171–213.

Gower ST, Vogt KA, Grier CC. 1992. Carbon dynamics of rocky mountain Douglas-fir: influence of water and nutrient availability. *Ecological Monographs* 62: 43–65.

Guswa AJ. 2008. The influence of climate on root depth: a carbon cost-benefit analysis. *Water Resources Research* 44: W02427.

Hari P, Mäkelä A, Korpilahti E, Holmberg M. 1986. Optimal control of gas exchange. *Tree Physiology* 2: 169–175.

Hartmann H. 2015. Carbon starvation during drought-induced tree mortality – are we chasing a myth? *Journal of Plant Hydraulics* 2: e005.

Hayat A, Hacket-Pain AJ, Pretzsch H, Rademacher TT, Friend AD. 2017. Modeling tree growth taking into account carbon source and sink limitations. *Frontiers in Plant Science* 8: 182.

Helmisaari HS, Siltala T. 1989. Variation in nutrient concentrations of Pinus sylvestris stems. *Scandinavian Journal of Forest Research* 4: 443–451.

Högberg P, Nordgren A, Ågren GI. 2002. Carbon allocation between tree root growth and root respiration in boreal pine forest. *Oecologia* 132: 579–581.

Hölttä T, Kurppa M, Nikinmaa E. 2013. Scaling of xylem and phloem transport capacity and resource usage with tree size. *Frontiers in Plant Science* 4: 496.

Hu M, Lehtonen A, Minunno F, Mäkelä A. 2020. Age effect on tree structure and biomass allocation in Scots pine (*Pinus sylvestris L.*) and Norway spruce (*Picea abies* [L.] *Karst.*). *Annals of Forest Science* 77: 1–15.

Imada S, Yamanaka N, Tamai S. 2008. Water table depth affects *Populus alba* fine root growth and whole plant biomass. *Functional Ecology* 22: 1018–1026.

Irvine J, Grace J. 1997. Continuous measurements of water tensions in the xylem of trees based on the elastic properties of wood. *Planta* 202: 455–461.

Ivanov VY, Bras RL, Vivoni ER. 2008. Vegetation-hydrology dynamics in complex terrain of semiarid areas: 1. A mechanistic approach to modeling dynamic feedbacks. *Water Resources Research* 44.

Iversen CM. 2010. Digging deeper: fine-root responses to rising atmospheric CO_2 concentration in forested ecosystems. *New Phytologist* 186: 346–357.

Jackson RB, Cook CW, Pippen JS, Palmer SM. 2009. Increased belowground biomass and soil CO_2 fluxes after a decade of carbon dioxide enrichment in a warm-temperate forest. *Ecology* 90: 3352–3366.

Janssens IA, Sampson DA, Cermak J, Meiresonne L, Riguzzi F, Overloop S, Ceulemans R. 1999. Above-and belowground phytomass and carbon storage in a Belgian Scots pine stand. *Annals of Forest Science* 56: 81–90.

Jiménez E, Moreno F, Peñuel M, Patino S, Lloyd J. 2009. Fine root dynamics for forests on contrasting soils in the Colombian Amazon. *Biogeosciences* 6: 2809–2827.

Kalnay E, Kanamitsu M, Kistler R, Collins W, Deaven D, Gandin L, Iredell M, Saha S, White G, Woollen J *et al.* 1996. The NCEP/NCAR 40-year reanalysis project. *Bulletin of the American Meteorological Society* 77: 437–472.

Katul G, Manzoni S, Palmroth S, Oren R. 2010. A stomatal optimization theory to describe the effects of atmospheric CO_2 on leaf photosynthesis and transpiration. *Annals of Botany* 105: 431–442.

King DA. 1990. The adaptive significance of tree height. *American Naturalist* 135: 809–828.

Kleidon A, Heimann M. 1996. Simulating root carbon storage with a coupled carbon—Water cycle root model. *Physics and Chemistry of the Earth* 21: 499–502.

Kolari P, Chan T, Porcar-Castell A, Bäck J, Nikinmaa E, Juurola E. 2014. Field and controlled environment measurements show strong seasonal acclimation in photosynthesis and respiration potential in boreal Scots pine. *Frontiers in Plant Science* 5: 717.

Laio F, D'Odorico P, Ridolfi L. 2006. An analytical model to relate the vertical root distribution to climate and soil properties. *Geophysical Research Letters* 33: L18401.

Lampurlanés J, Cantero-Martínez C. 2006. Hydraulic conductivity, residue cover and soil surface roughness under different tillage systems in semiarid conditions. *Soil and Tillage Research* 85: 13–26.

Landsberg JJ, Blanchard TW, Warrit B. 1976. Studies on movement of water through apple-trees. *Journal of Experimental Botany* 27: 579–596.

Lawrence DM, Fisher RA, Koven CD, Oleson KW, Swenson SC, Bonan G, Collier N, Ghimire B, Kampenhout L, Kennedy D *et al.* 2019. The Community Land Model version 5: Description of new features, benchmarking, and impact of forcing uncertainty. *Journal of Advances in Modeling Earth Systems* 11: 4245–4287.

Le Quéré C, Andrew RM, Friedlingstein P, Sitch S, Hauck J, Pongratz J, Pickers PA, Korsbakken JI, Peters GP, Canadell JG *et al.* 2018. Global carbon budget 2018. *Earth System Science Data* 10: 2141–2194.

Ledo A, Paul KI, Burslem DF, Ewel JJ, Barton C, Battaglia M, Brooksbank K, Carter J, Eid TH, England JR *et al.* 2018. Tree size and climatic water deficit control root to shoot ratio in individual trees globally. *New Phytologist* 217: 8–11.

Litton CM. 2002. *Above- and belowground carbon allocation in post-fire lodgepole pine forests: effects of tree density and stand age*. Laramie, WY, USA: Department of Botany, University of Wyoming, 210.

Litton CM, Raich JW, Ryan MG. 2007. Carbon allocation in forest ecosystems. *Global Change Biology* 13: 2089–2109.

Love DM, Venturas MD, Sperry JS, Brooks PD, Pettit JL, Wang Y, Anderegg WRL, Tai X, Mackay DS. 2019. Dependence of aspen stands on a subsurface water subsidy: implications for climate change impacts. *Water Resources Research* 55: 1833–2184.

Mackay DS, Savoy PR, Grossiord C, Tai X, Pleban JR, Wang DR, McDowell NG, Adams HD, Sperry JS. 2020. Conifers depend on established roots during drought: results from a coupled model of carbon allocation and hydraulics. *New Phytologist* 225: 679–692.

Magnani F, Mencuccini M, Grace J. 2000. Age-related decline in stand productivity: the role of structural acclimation under hydraulic constraints. *Plant, Cell & Environment* 23: 251–263.

Mäkelä A, Berninger F, Hari P. 1996. Optimal control of gas exchange during drought: theoretical analysis. *Annals of Botany* 77: 461–468.

Mäkelä A, Givnish TJ, Berninger F, Buckley TN, Farquhar GD, Hari P. 2002. Challenges and opportunities of the optimality approach in plant ecology. *Silva Fennica* 36: 605–614.

Mäkelä A, Sievanen RP. 1987. Comparison of two shoot-root partitioning models with respect to substrate utilization and functional balance. *Annals of Botany* 59: 129–140.

Mäkelä A, Valentine HT, Helmisaari HS. 2008. Optimal co-allocation of carbon and nitrogen in a forest stand at steady state. *New Phytologist* 180: 114–123.

Manzoni S, Vico G, Katul G, Fay PA, Polley W, Palmroth S, Porporato A. 2011. Optimizing stomatal conductance for maximum carbon gain under water stress: a meta-analysis across plant functional types and climates. *Functional Ecology* 25: 456–467.

Martínez-Vilalta J, Cochard H, Mencuccini M, Sterck F, Herrero A, Korhonen JFJ, Llorens P, Nikinmaa E, Nolè A, Poyatos R *et al.* 2009. Hydraulic adjustment of Scots pine across Europe. *New Phytologist* 184: 353–364.

Martínez-Vilalta J, Korakaki E, Vanderklein D, Mencuccini M. 2007. Below-ground hydraulic conductance is a function of environmental conditions and tree size in Scots pine. *Functional Ecology* 21: 1072–1083.

McLaughlin BC, Ackerly DD, Klos PZ, Natali J, Dawson TE, Thompson SE. 2017. Hydrologic refugia, plants, and climate change. *Global Change Biology* 23: 2941–2961.

McLaughlin BC, Blakey R, Weitz AP, Feng X, Brown BJ, Ackerly DD, Dawson TE, Thompson SE. 2020. Weather underground: Subsurface hydrologic processes mediate tree vulnerability to extreme climatic drought. *Global Change Biology* **26**: 3091–3107.

McMahon TA. 1973. Size and shape in biology. *Science* **179**: 1201–1204.

McMurtrie RE, Norby RJ, Medlyn BE, Dewar RC, Pepper DA, Reich PB, Barton CV. 2008. Why is plant-growth response to elevated CO_2 amplified when water is limiting, but reduced when nitrogen is limiting? A growth-optimisation hypothesis. *Functional Plant Biology* **35**: 521–534.

Meir P, Kruijt B, Broadmeadow M, Barbosa E, Kull O, Carswell F, Nobre A, Jarvis PG. 2002. Acclimation of photosynthetic capacity to irradiance in tree canopies in relation to leaf nitrogen concentration and leaf mass per unit area. *Plant, Cell & Environment* **25**: 343–357.

Mencuccini M, Grace J. 1994. Climate influences the leaf area/sapwood area ratio in Scots pine. *Tree Physiology* **15**: 1–10.

Mencuccini M, Grace J. 1996. Hydraulic conductance, light interception and needle nutrient concentration in Scots pine stands and their relations with net primary productivity. *Tree Physiology* **16**: 459–468.

Mencuccini M, Martínez-Vilalta J, Vanderklein D, Hamid HA, Korakaki E, Lee S, Michiels B. 2005. Size-mediated ageing reduces vigour in trees. *Ecology letters* **8**: 1183–1190.

Merganičová K, Merganič J, Lehtonen A, Vacchiano G, Sever MZO, Augustynczik AL, Grote R, Kyselová I, Mäkelä A, Yousefpour R et al. 2019. Forest carbon allocation modelling under climate change. *Tree Physiology* **39**: 1937–1960.

Morison JIL. 1987. Intercellular CO_2 concentration and stomatal response to CO_2. In: Zeiger E, Cowan IR, Farquhar GD, eds. *Stomatal function.* Stanford, CA, USA: Stanford University Press, 229–251.

Naumburg E, Mata-Gonzalez R, Hunter RG, McLendon T, Martin DW. 2005. Phreatophytic vegetation and groundwater fluctuations: A review of current research and application of ecosystem response modeling with an emphasis on great basin vegetation. *Environmental Management* **35**: 726–740.

Nikinmaa E, Hölttä T, Hari P, Kolari P, Mäkelä A, Sevanto S, Vesala T. 2013. Assimilate transport in phloem sets conditions for leaf gas exchange. *Plant, Cell & Environment* **36**: 655–669.

Niklas KJ, Spatz HC. 2004. Growth and hydraulic (not mechanical) constraints govern the scaling of tree height and mass. *Proceedings of the National Academy of Sciences, USA* **101**: 15661–15663.

Norby RJ, Wullschleger SD, Hanson PJ, Gunderson CA, Tschaplinski TJ, Jastrow JD. 2006. CO_2 enrichment of a deciduous forest: the Oak Ridge FACE experiment. In: Nösberger J, Long SP, Norby RJ, Stitt M, Hendrey GR, Blum H, eds. *Managed Ecosystems and CO_2.* Berlin/Heidelberg, Germany: Springer, 231–251.

Novick KA, Ficklin DL, Stoy PC, Williams CA, Bohrer G, Oishi AC, Papuga SA, Blanken PD, Noormets A, Sulman BN. 2016b. The increasing importance of atmospheric demand for ecosystem water and carbon fluxes. *Nature Climate Change* **6**: 1023–1027.

Novick KA, Miniat CF, Vose JM. 2016a. Drought limitations to leaf-level gas exchange: results from a model linking stomatal optimization and cohesion–tension theory. *Plant, Cell & Environment* **39**: 583–596.

Oleksyn J, Reich PB, Chalupka W, Tjoelker MG. 1999. Differential above-and below-ground biomass accumulation of European *Pinus sylvestris* populations in a 12-year-old provenance experiment. *Scandinavian Journal of Forest Research* **14**: 7–17.

Oleson KW, Lawrence DM, Gordon B, Flanner MG, Kluzek E, Peter J, Heald CL. 2010. *Technical description of version 4.0 of the Community Land Model (CLM).* Note. NCAR/TN-4781STR. Boulder, CO, USA: NCAR Technical Note.

Oleson KW, Lawrence DM, Bonan GB, Drewniak B, Huang M, Koven CD, Swenson SC. 2013. *Technical description of version 4.5 of the community land model (CLM),* Note. NCAR/TN-503+ STR. Boulder, CO, USA: NCAR Technical Note.

Onoda Y, Saluña JB, Akutsu K, Aiba SI, Yahara T, Anten NP. 2014. Trade-off between light interception efficiency and light use efficiency: implications for species coexistence in one-sided light competition. *Journal of Ecology* **102**: 167–175.

Pan Y, Birdsey RA, Fang J, Houghton R, Kauppi PE, Kurz WA, Phillips OL, Shvidenko A, Lewis SL, Canadell JG et al. 2011. A large and persistent carbon sink in the World's forests. *Science* **333**: 988–993.

Penman HL. 1948. Natural evaporation from open water, bare soil and grass. *Proceedings of the Royal Society of London Series A: Mathematical and Physical Sciences* **193**, 1032, 120–145.

Persson H. 1980. Fine root dynamics in a Scots pine stand with and without near optimum nutrient and water regimes. *Acta Phytogeographica Suecica* **68**: 101–110.

Poorter H, Jagodzinski AM, Ruiz-Peinado R, Kuyah S, Luo Y, Oleksyn J, Usoltsev VA, Buckley TN, Reich PB, Sack L. 2015. How does biomass distribution change with size and differ among species? An analysis for 1200 plant species from five continents. *New Phytologist* **208**: 736–749.

Poorter H, Nagel O. 2000. The role of biomass allocation in the growth response of plants to different levels of light, CO_2, nutrients and water: a quantitative review. *Functional Plant Biology* **27**: 1191.

Poorter H, Niklas KJ, Reich PB, Oleksyn J, Poot P, Mommer L. 2012. Biomass allocation to leaves, stems and roots: meta-analyses of interspecific variation and environmental control. *New Phytologist* **193**: 30–50.

Poyatos R, Aguadé D, Galiano L, Mencuccini M, Martínez-Vilalta J. 2013. Drought-induced defoliation and long periods of near-zero gas exchange play a key role in accentuating metabolic decline of Scots pine. *New Phytologist* **200**: 388–401.

Poyatos R, Aguadé D, Martínez-Vilalta J. 2018. Below-ground hydraulic constraints during drought-induced decline in Scots pine. *Annals of Forest Science* **75**: 100.

Poyatos R, Martínez-Vilalta J, Čermák J, Ceulemans R, Granier A, Irvine J, Köstner B, Lagergren F, Meiresonne L, Nadezhdina N, Zimmermann R, Llorens P, Mencuccini M. 2007. Plasticity in hydraulic architecture of Scots pine across Eurasia. *Oecologia* **153**: 245–259.

Pretzsch H. 2014. Canopy space filling and tree crown morphology in mixed-species stands compared with monocultures. *Forest Ecology and Management* **327**: 251–264.

Pritchard SG, Strand AE, McCORMACK ML, Davis MA, Finzi AC, Jackson RB, Matamala R, Rogers HH, Oren R. 2008. Fine root dynamics in a loblolly pine forest are influenced by free-air-CO_2 -enrichment: a six-year-minirhizotron study. *Global Change Biology* **14**: 588–602.

Reid CPP, Odegard GJ, Hokenstrom JC, McConnell WJ, Frayer WE. 1974. *Effects of clearcutting on nutrient cycling in lodgepole pine forests.* Fort Collins, CO, USA: Colorado State University and United States Forest Service, 321.

Reyer CPO, Silveyra Gonzalez R, Dolos K, Hartig F, Hauf Y, Noack M, Lasch-Born P, Rötzer T, Pretzsch H, Meesenburg H et al. 2020. The PROFOUND Database for evaluating vegetation models and simulating climate impacts on European forests. *Earth System Science Data* **12**: 1295–1320.

Reynolds JF, Thornley JHM. 1982. A shoot:root partitioning model. *Annals of Botany* **49**: 585–597.

Richards LA. 1931. Capillary conduction of liquids through porous medium. *Physics* **1**: 318–333.

Richardson LF. 1922. *Weather prediction by numerical process.* Cambridge, UK: University Press, 262.

Roberts J. 1977. Use of tree-cutting techniques in study of water relations of mature *Pinus sylvestris* L.1. Technique and survey of results. *Journal of Experimental Botany* **28**: 751–767.

Roebroek CT, Melsen LA, Hoek van Dijke AJ, Fan Y, Teuling AJ. 2020. Global distribution of hydrologic controls on forest growth. *Hydrology and Earth System Sciences* **24**: 4625–4639.

Rosas T, Mencuccini M, Barba J, Cochard H, Saura-Mas S, Martínez-Vilalta J. 2019. Adjustments and coordination of hydraulic, leaf and stem traits along a water availability gradient. *New Phytologist* **223**: 632–646.

Running SW. 1980. Field estimates of root and xylem resistances in *Pinus contorta* using root excision. *Journal of Experimental Botany* **31**: 555–569.

Ryan MG. 1989. Sapwood volume for three subalpine conifers: predictive equations and ecological implications. *Canadian Journal of Forest Research* **19**: 1397–1401.

Sabine CL, Heimann M, Artaxo P, Bakker DC, Chen CTA, Field CB, Gruber, N, Le Quere, C, Prinn, RG, Richey, JE, Lankao, PR, Sathaye, JA & Vallentini, R. 2004. Current status and past trends of the global carbon cycle.

Scope-scientific Committee on Problems of the Environment International Council of Scientific Unions 62: 17–44.

Sabot ME, De Kauwe MG, Pitman AJ, Medlyn BE, Verhoef A, Ukkola AM, Abramowitz G. 2020. Plant profit maximization improves predictions of European forest responses to drought. *New Phytologist* 226: 1638–1655.

Savage VM, Bentley LP, Enquist BJ, Sperry JS, Smith DD, Reich PB, Von Allmen EI. 2010. Hydraulic trade-offs and space filling enable better predictions of vascular structure and function in plants. *Proceedings of the National Academy of Sciences, USA* 107: 22722–22727.

Schenk HJ. 2008. The shallowest possible water extraction profile: a null model for global root distributions. *Vadose Zone Journal* 7: 1119–1124.

Schenk HJ, Jackson RB. 2002. Rooting depths, lateral root spreads and below-ground/above-ground allometries of plants in water-limited ecosystems. *Journal of Ecology* 480–494.

Schenk HJ, Jackson RB. 2005. Mapping the global distribution of deep roots in relation to climate and soil characteristics. *Geoderma* 126: 129–140.

Schiestl-Aalto P, Kulmala L, Mäkinen H, Nikinmaa E, Mäkelä A. 2015. CASSIA–a dynamic model for predicting intra-annual sink demand and interannual growth variation in Scots pine. *New Phytologist* 206: 647–659.

Schimel D, Stephens BB, Fisher JB. 2015. Effect of increasing CO_2 on the terrestrial carbon cycle. *Proceedings of the National Academy of Sciences, USA* 112: 436–441.

Schwinning S, Ehleringer JR. 2001. Water use trade-offs and optimal adaptations to pulse-driven arid ecosystems. *Journal of Ecology* 89: 464–480.

Schymanski SJ, Sivapalan M, Roderick ML, Beringer J, Hutley LB. 2008. An optimality-based model of the coupled soil moisture and root dynamics. *Hydrology and Earth System Sciences* 12: 913–932.

Schymanski SJ, Sivapalan M, Roderick ML, Hutley LB, Beringer J. 2009. An optimality-based model of the dynamic feedbacks between natural vegetation and the water balance. *Water Resources Research* 45: WO1412.

Sendròs A, Diaz Y, Himi M, Tapias JC, Rivero L, Font X, Casas A. 2014. An evaluation of aquifer vulnerability in two nitrate sensitive areas of Catalonia (NE Spain) based on electrical resistivity methods. *Environmental Earth Sciences* 71: 77–84.

Shao J, Si B, Jin J. 2019. Rooting depth and extreme precipitation regulate groundwater recharge in the thick unsaturated zone: A case study. *Water* 11: 1232.

Shinozaki K, Yoda K, Hozumi K, Kira T. 1964. A quantitative analysis of plant form-the pipe model theory: I. Basic analyses. *Japanese Journal of Ecology* 14: 97–105.

Sivandran G, Bras RL. 2013. Dynamic root distributions in ecohydrological modeling: A case study at Walnut Gulch Experimental Watershed. *Water Resources Research* 49: 3292–3305.

Sperry JS, Love DM. 2015. Tansley review: What plant hydraulics can tell us about plant responses to climate-change droughts. *New Phytologist* 207: 14–27.

Sperry JS, Smith DD, Savage VM, Enquist BJ, McCulloh KA, Reich PB, Bentley LP, von Allmen EI. 2012. A species-level model for metabolic scaling in trees I. Exploring boundaries to scaling space within and across species. *Functional Ecology* 26: 1054–1065.

Sperry JS, Venturas MD, Anderegg WR, Mencuccini M, Mackay DS, Wang Y, Love DM. 2017. Predicting stomatal responses to the environment from the optimization of photosynthetic gain and hydraulic cost. *Plant, Cell & Environment* 40: 816–830.

Sperry JS, Venturas MD, Todd HN, Trugman AT, Anderegg WR, Wang Y, Tai X. 2019. The impact of rising CO_2 and acclimation on the response of US forests to global warming. *Proceedings of the National Academy of Sciences, USA* 116: 25734–25744.

Sperry JS, Wang Y, Wolfe B, Mackay DS, Anderegg WRL, McDowell NG, Pockman WT. 2016. Pragmatic hydraulic theory predicts stomatal responses to climatic water deficits. *New Phytologist* 212: 577–589.

Stulen I, Den Hertog J. 1993. Root growth and functioning under atmospheric CO_2 enrichment. *Vegetatio* 104: 99–115.

Sus O, Poyatos R, Barba J, Carvalhais N, Llorens P, Williams M, Vilalta J. 2014. Time variable hydraulic parameters improve the performance of a mechanistic stand transpiration model. A case study of Mediterranean Scots pine sap flow data assimilation. *Agricultural & Forest Meteorology* 198–199: 168–180.

Tai X, Mackay DS, Sperry JS, Brooks P, Anderegg WRL, Flanagan LB, Rood SB, Hopkinson C. 2018. Distributed plant hydraulic and hydrological modeling to understand the susceptibility of riparian woodland trees to drought-induced mortality. *Water Resources Research* 54: 4901–4915.

Thornley JH, Parsons AJ. 2014. Allocation of new growth between shoot, root and mycorrhiza in relation to carbon, nitrogen and phosphate supply: teleonomy with maximum growth rate. *Journal of Theoretical Biology* 342: 1–14.

Torres-Ruiz JM, Cochard H, Mencuccini M, Delzon S, Badel E. 2016. Direct observation and modelling of embolism spread between xylem conduits: a case study in Scots pine. *Plant, Cell & Environment* 39: 2774–2785.

Trugman AT, Anderegg LD, Sperry JS, Wang Y, Venturas M, Anderegg WR. 2019a. Leveraging plant hydraulics to yield predictive and dynamic plant leaf allocation in vegetation models with climate change. *Global Change Biology* 25: 4008–4021.

Trugman AT, Anderegg LDL, Wolfe BT, Birami B, Ruehr NK, Detto M, Bartlett MK, Anderegg WRL. 2019. Climate and plant trait strategies determine tree carbon allocation to leaves and mediate future forest productivity. *Global Change Biology* 25: 3395–3405.

Tsuda M, Tyree MT. 1997. Whole-plant hydraulic resistance and vulnerability segmentation in *Acer saccharinum*. *Tree Physiology* 17: 351–357.

Van Wijk MT, Bouten W. 2001. Towards understanding tree root profiles: simulating hydrologically optimal strategies for root distribution. *Hydrology and Earth System Sciences Discussions, European Geosciences Union* 2001: 629–644.

Venturas MD, Sperry JS, Love DM, Frehner EH, Allred MG, Wang Y, Anderegg WR. 2018. A stomatal control model based on optimization of carbon gain vs hydraulic risk predicts aspen sapling responses to drought. *New Phytologist* 220: 836–850.

Wang Y, Sperry JS, Venturas MD, Trugman AT, Love DM, Anderegg WR. 2019. The stomatal response to rising CO_2 concentration and drought is predicted by a hydraulic trait-based optimization model. *Tree Physiology* 39: 1416–1427.

Wang Y, Sperry JS, Anderegg WR, Venturas MD, Trugman AT. 2020. A theoretical and empirical assessment of stomatal optimization modeling. *New Phytologist* 227: 311–325.

West GB, Brown JH, Enquist BJ. 1999. A general model for the structure and allometry of plant vascular systems. *Nature* 400: 664–667.

West GB, Enquist BJ, Brown JH. 2009. A general quantitative theory of forest structure and dynamics. *Proceedings of the National Academy of Sciences, USA* 106: 7040–7045.

Wolf A, Anderegg WR, Pacala SW. 2016. Optimal stomatal behavior with competition for water and risk of hydraulic impairment. *Proceedings of the National Academy of Sciences, USA* 113: E7222–E7230.

Xia J, Yuan W, Lienert S, Joos F, Ciais P, Viovy N, Wang Y, Wang X, Zhang H, Chen Y *et al.* 2019. Global patterns in net primary production allocation regulated by environmental conditions and forest stand age: a model-data comparison. *Journal of Geophysical Research: Biogeosciences* 124: 2039–2059.

Xu GQ, Yu DD, Li Y. 2017. Patterns of biomass allocation in *Haloxylon persicum* woodlands and their understory herbaceous layer along a groundwater depth gradient. *Forest Ecology and Management* 395: 37–47.

Yang J, Medlyn BE, De Kauwe MG, Duursma RA. 2018. Applying the concept of ecohydrological equilibrium to predict steady state leaf area index. *Journal of Advances in Modeling Earth Systems* 10: 1740–1758.

Zha T, Kellomäki S, Wang KY, Ryyppö A, Niinistö S. 2004. Seasonal and annual stem respiration of Scots pine trees under boreal conditions. *Annals of Botany* 94: 889–896.

Zolfaghar S, Villalobos-Vega R, Cleverly J, Zeppel M, Rumman R, Eamus D. 2014. The influence of depth-to-groundwater on structure and productivity of Eucalyptus woodlands. *Australian Journal of Botany* 62: 428–437.

Zolfaghar S, Villalobos-Vega R, Zeppel M, Eamus D. 2015. The hydraulic architecture of Eucalyptus trees growing across a gradient of depth-to-groundwater. *Functional Plant Biology* 42: 888–898.

Supporting Information

Additional Supporting Information may be found online in the Supporting Information section at the end of the article.

Fig. S1 Comparison optimal/numerical and gradient ascent approximation for optimization of arbitrary fitness surfaces.

Fig. S2 Comparison of optimal allocation methods predicted numerically and by THORP's approximation.

Fig. S3 Comparison of observed and THORP-predicted leaf water potentials for the Poblet Forest Natural Reserve site.

Fig. S4 Root-to-shoot ratios simulated by control experiment.

Fig. S5 LAI and leaf- and sapwood-area relations under reduced air humidity.

Fig. S6 Rooting depth and indices of water stress simulated by control experiment.

Fig. S7 Rooting depth and indices of water stress simulated by experiment with reduced (75%) precipitation.

Fig. S8 Rooting depth and indices of water stress simulated by experiment with further reduced (50%) precipitation.

Fig. S9 Rooting depth and indices of water stress simulated by experiment with further reduced (50%) precipitation and a shallow, 2-m-deep groundwater table.

Fig. S10 Measures of water stress and productivity from the eCO_2 experiment.

Fig. S11 Shoot-to-root biomass ratio and total biomass from pruning experiments.

Fig. S12 Flowchart of model computations.

Fig. S13 Model–observation comparison for the tree size dependence of stem hydraulic conductance.

Table S1 Main variables in THORP.

Notes S1 Full model and simulation descriptions.

Notes S2 MATLAB code for model and plotting/analyzing data, including forcing data and simulation outputs.

Please note: Wiley-Blackwell are not responsible for the content or functionality of any supporting information supplied by the authors. Any queries (other than missing material) should be directed to the *New Phytologist* Central Office.